

November 1, 1996
VERSION 3.0

**Algorithm Theoretical Basis Document (ATBD) for
the MODIS Snow-, Lake Ice- and Sea Ice-Mapping
Algorithms**

Dorothy K. Hall
Associate MODIS Team Member
Hydrological Sciences Branch
NASA/Goddard Space Flight Center
Greenbelt, MD 20771

George A. Riggs
Scientist/Programmer
Research and Data Systems Corporation
7833 Walker Drive, Suite 550
Greenbelt, MD 20770

Vincent V. Salomonson
MODIS Team Member
Earth Sciences Directorate
NASA/Goddard Space Flight Center
Greenbelt, MD 20771

With contributions from:

Janet Y.L. Chien
Programmer/Analyst
General Sciences Corporation
6100 Chevy Chase Drive
Laurel, MD 20707

Andrew Klein
Scientist
General Sciences Corporation
6100 Chevy Chase Drive
Laurel, MD 20707

Alexandra Moore
Dept. of Geological and Environmental Sciences
Hartwick College
Oneonta, NY 13820

Table of Contents

Executive Summary

1.0	Introduction.....	5
1.1	Experimental Objective.....	6
1.2	Algorithm Implementation.....	7
2.0	Background.....	8
2.1	Remote Sensing of Snow Cover.....	8
2.2	Remote Sensing of Ice on Large Inland Lakes.....	9
2.3	Remote Sensing of Sea Ice Cover.....	10
3.0	MODIS Instrument Characteristics.....	12
4.0	Algorithm Descriptions.....	14
4.1	Philosophy Behind Selection of Algorithms.....	14
4.2	SNOMAP.....	15
4.2.1	Normalized Difference Snow Index (NDSI).....	16
4.2.2	Use of Reflectances for Calculation of NDSI.....	17
4.2.3	Estimate of Global Errors in Snow.....	17
4.2.3.1	Mapping Snow cover in densely-forested.....	18
4.2.3.2	Snow/Cloud Discrimination.....	21
4.2.3.3	Variation of Reflectance due to View Angle.....	22
4.3	Lake Ice.....	24
4.4	ICEMAP.....	24
4.4.1	Development of ICEMAP.....	24
4.4.2	Detection of Sea Ice.....	24
4.4.3	Ice Surface Temperature (IST) Algorithm.....	25
4.4.4	Ice/Cloud Discrimination.....	27
4.4.5	Sources of Error.....	27
4.5	Gridding of Snow and Sea Ice Products.....	28

5.0	Validation.....	28
5.1	Pre-Launch Validation Activities.....	29
5.1.1	Snow.....	29
5.1.1.1	Comparison with Sierra Nevada TM Scene.....	29
5.1.1.2	BOREAS Experiment/February 1994.....	32
5.1.1.3	April 1995 Alaska Experiment.....	32
5.1.1.4	New England/Wisconsin Mission/Jan & Feb 1997.....	32
5.1.1.5	Validation of SNOMAP using Supervised.....	33
5.1.2	Sea Ice.....	34
5.2	Post-Launch Validation Activities.....	34
5.2.1	Snow.....	34
5.2.1.2	Comparison with other Global-Scale Products.....	34
5.2.2	Sea Ice.....	35
6.0	Combination of MODIS and other EOS data.....	35
6.1	Preliminary Analysis of Snow Cover in Alaska.....	36
7.0	References.....	39
8.0	Figure Captions.....	45
9.0	Appendix A: Product Level Definitions.....	48
	Appendix B: Response to Reviewers' Comments.....	49

EXECUTIVE SUMMARY

Algorithms are currently under development to map snow cover (including ice on large, inland lakes), sea ice cover, and sea ice surface temperature (IST), using future Earth Observation System (EOS) Moderate Resolution Imaging Spectroradiometer (MODIS) data. The Level-3 products (digital maps) will provide daily and 10-day composites of global snow and lake ice cover at 500-m resolution, and sea ice cover and IST at 1-km resolution. Statistics will be provided regarding the extent and persistence of snow and ice cover at each grid cell for the Level-3 products. The snow

(SNOMAP) and sea ice (ICEMAP) mapping algorithms employ a Normalized Difference Snow Index (NDSI) to identify and classify snow and ice on a pixel-by-pixel basis. SNOMAP and ICEMAP employ the land/water mask and the MODIS cloud mask to define the areas of interest. Then the MODIS surface reflectance product is used as input. The usefulness of the NDSI is based on the fact that snow and ice are considerably more reflective in the visible than in the short-wave IR part of the spectrum, and the reflectance of some clouds remains high in the short-wave IR, while the reflectance of snow is low. MODIS snow and ice products will be archived at the National Snow and Ice Data Center (NSIDC) Distributed Active Archive Center (DAAC), located in Boulder, Colorado.

Validation of the SNOMAP and ICEMAP algorithms is being undertaken in the pre-launch time frame and will be continued in the post-launch time frame. Current validation efforts show that on a TM scene of the snow-covered Sierra Nevada Mountains in California, SNOMAP has >98 percent accuracy in mapping snow cover for pixels that contain about 50-60 percent or more snow cover. For pixels that contain <50 percent snow cover, the accuracy is less. SNOMAP has been run on approximately 25 other TM scenes. Because snow mapping in densely-forested areas represents a limitation to snow mapping, we must determine error bars for mapping snow in these areas of the world.

The accuracy of the MODIS snow maps will vary with land-cover type; the SNOMAP algorithm has been and will continue to be tested in a variety of land covers. Errors have been or will be determined for the following land covers: agricultural, alpine, forested, prairie and tundra areas. This will be done using a series of focused field and aircraft experiments. These errors will be extrapolated to the global scale at least initially, to gain quantitative insight into global-scale errors to be expected using SNOMAP. A global error estimate will be made by determining errors in each of the different land covers, weighted by the percent of that particular land cover in the snow-covered areas globally. Error estimates will be refined in the post-launch time frame, at which time it will be possible to use the MODIS at-launch land-cover product to identify classes of land cover globally.

The MODIS snow and ice products will be validated in relationship to EOS and non-EOS snow data sets, as well as ground observations. Focused aircraft and field campaigns have been undertaken in order to validate SNOMAP and ICEMAP. Aircraft and field experiments have been conducted in forested areas of Montana, Saskatchewan and Alaska, and over prairies in Montana, and tundra in Alaska, and over sea ice in the Bering and Beaufort Seas off the coasts of Alaska. The MODIS Airborne Simulator (MAS) has been flown in Saskatchewan and Alaska. Additional campaigns are planned to

validate the snow and ice maps and IST using ground and aircraft data in the pre- and post-launch time frame. Specifically, a field and aircraft experiment is planned in conjunction with other MODIS investigators in Wisconsin and New Hampshire for January and February 1997. Additional post-launch validation activities will be undertaken in key areas of interest.

For post-launch validation of river-basin scale areas, Landsat-7 Enhanced Thematic Mapper+ (ETM+) and EOS Advanced Spaceborne Thermal Emission and Reflection Radiometer (ASTER) data will also be used following the launch of the first EOS-AM spacecraft. For post-launch validation at the hemispheric scale, NOAA/NESDIS snow and sea ice maps will be available for comparison. NOAA National Operational Hydrologic Remote Sensing Center (NOHRSC)-derived regional maps are now available, and in the future will be available for comparison with the MODIS maps. Advanced Microwave Scanner Radiometer (AMSR)-derived snow and ice maps will be available (in 2000 and beyond).

Only in the post-launch time frame will it be possible to determine the full capabilities of the MODIS for snow and sea ice mapping because the unique combination of MODIS spectral bands has not been available on a satellite prior to MODIS. Also in the post-launch time period, and, after the launch of the EOS-PM spacecraft, the potential exists for combining MODIS, Multi-Angle Imaging Spectro-Radiometer (MISR) and Advanced Microwave Sounder Radiometer (AMSR) data products to generate an enhanced snow product. It is envisioned that a product can be developed that will employ reflective and passive-microwave data that will permit snow extent, albedo and depth to be mapped, thus enabling daily maps to be generated irrespective of cloud cover and darkness.

1.0 INTRODUCTION

The purpose of the MODIS snow mapping (SNOMAP) and ice mapping (ICEMAP) algorithms is to generate global snow- and lake-ice cover products, and global sea ice-cover products from MODIS data. The SNOMAP algorithm is based on ratioing techniques that have been proven to be successful at local and regional scales. Results herein show that the technique can be applied globally. Daily snow and ice maps and maximum 10-day snow and lake ice cover, snow-covered area (i.e. hemispheric snowline), and daily and maximum 10-day composited sea ice-cover and sea ice surface temperature (IST) Level-3 digital-map products will be generated in the Product Generation System (PGS) of the Earth Observation System Data Information System (EOSDIS) (Figures 1 and 2). Users may access the products using the services of EOSDIS. Snow and ice products will be archived at and distributed from the National Snow and Ice Data Center (NSIDC) Distributed Active Archive Center (DAAC) at the University of Colorado in Boulder, Colorado.

The MODIS snow maps will augment the valuable record of Northern Hemisphere snow cover that was started in 1966 by NOAA (Matson et. al., 1986). The numerous spectral bands and superior spatial resolution of MODIS, relative to the Advanced Very High Resolution Radiometer (AVHRR), will permit an improved ability to map snow and ice. The MODIS snow-cover product will be an advancement over the NOAA maps because MODIS-derived maps will be able to provide snow maps at 500-m spatial resolution (versus 25-km resolution for the NOAA product); also, daily as well as composited maps will be produced from MODIS data. And, the MODIS product development will be automated thus reducing or eliminating errors due to human subjectivity. Statistics concerning snow-cover persistence and duration using the 10-day composites will be generated. Furthermore, additional snow-cover information on pixels that are 50-60 percent snow covered may be able to be provided with the MODIS maps if a reasonable threshold can be identified after analysis of data in a variety of land covers.

The sea ice maps will augment the record of sea ice cover that is produced by NOAA. Currently, there is no IST product generated on a regular basis from satellites. Therefore, the MODIS IST product will represent an important advance for the sea ice and global modeling communities.

SNOMAP and ICEMAP will identify snow, lake ice and sea ice by their reflectance or emittance properties. SNOMAP consists of a series of criteria tests and decision rules that identifies snow and lake ice, if present, in each pixel of a MODIS image. SNOMAP will generate a data set of global snow cover and of ice cover on large, inland lakes at 500-m resolution. ICEMAP is structured in a similar fashion to

SNOMAP, for mapping daily and maximum 10-day composited sea ice cover globally at 1-km resolution. Also at 1-km resolution, IST will be mapped daily and average ice surface temperature will be mapped for 10-day periods, day and night.

The basic techniques used in the snow and ice mapping algorithms are threshold-based criteria tests, the normalized difference between bands, and decision rules. Use of the ratio of a short-wave IR channel to a visible channel was determined by Kyle et al. (1978) and Bunting and d'Entremont (1982) to be useful for snow-cover mapping, and later utilized by Dozier (1989) to map snow in the Sierra Nevada Mountains. This method is the basis for SNOMAP and ICEMAP. The basis of the IST algorithm is the work of Key and Collins (in press); the IST algorithm will employ two MODIS IR bands.

Expected errors will be determined quantitatively in the pre-launch time frame by determining snow-mapping errors in five land covers (agricultural, alpine, forest, prairie and tundra). These errors will be extrapolated to the global scale for a rough estimate of global-scale error in snow mapping using SNOMAP. In the post-launch time frame, use of the MODIS land-cover map will permit us to improve our error estimate, both in individual land covers and on the global scale. Using the MODIS land-cover map, we may also be able to determine a credible threshold value in forested areas that will enable more snow to be mapped in those areas.

Development of algorithms to map snow, lake ice and sea ice is an evolutionary process. The algorithms may change as input data and information improve, and in response to the results of validation studies. The algorithms are likely to change after MODIS Airborne Simulator (MAS) data are analyzed, and again after MODIS is launched. At that time, the full capabilities of the MODIS sensor can be utilized to optimize the derivation of snow, lake ice and sea ice cover and IST.

1.1 Experimental Objective

The snow, lake ice and sea ice products will be used to monitor the variability and trends in global snow and ice extent, and to determine duration of lake ice on large, inland lakes. Global snow cover and sea ice are important parameters in global energy balance; IST has a profound influence on sea ice growth, snow metamorphosis, and snow/ice melt (Key and Collins, in press). It has been shown that global climate models (GCMs) do not simulate the present Arctic climate very well (Bromwich et al., 1994); thus improved measurements of global snow and ice cover and other cryospheric elements are necessary to improve modeling scenarios.

The objective of this research is to develop and implement algorithms that will map snow and ice on a daily basis, and provide statistics about the extent and persistence of snow and ice cover over a 10-day period. The SNOMAP and ICEMAP output products will consist of daily data and data composited to create a digital map of maximum 10-day global snow, lake ice and sea ice extent (Level-3 product). [See Appendix A for definitions of product level descriptions.] Data will be gridded in a polar-stereographic projection for the Northern and Southern Hemispheres, then cast to a sinusoidal projection for snow and lake ice cover, and retained in the polar-stereographic projection for sea ice and IST maps. IST will also be mapped daily and average IST will be mapped in 10-day composites. Snow cover in pixels that are 50 - 60 percent or greater snow covered will be mapped.

MODIS-derived snow and sea ice extent will also be produced at $1/4^\circ \times 1/4^\circ$ resolution and will be available as input to GCMs. Also, at a typical GCM grid scale of 60×60 km, the 500-m resolution data will enable sub-pixel snow mapping for use in regional and global climate models. A snow-cover submodel can be used to take advantage of patchy snowmelt modeling developments (Liston, 1995). From the 500-m resolution snow product, snow-cover depletion curves for each model grid cell can be calculated (Glen Liston, oral communication, 1996). The generation of a methodology which directly accounts for the influence of subgrid-scale snow-cover variability, within the context of regional and global climate models, is expected to improve key features of the model-simulated Earth's radiation balance and land-surface hydrology.

A consistent record of ice conditions on large inland lakes will permit studies to be done on freeze-up and break-up dates of large lakes. These data can be correlated with regional meteorological conditions and will be useful in climate-change studies. Such a record, at 500-m resolution, may also be useful to operational ice mapping for navigation, but our planned maps are not designed for such an application because the time required to generate and distribute the EOS data following acquisition is likely to be greater than that required for operational use.

1.2 Algorithm Implementation

Expected MODIS data inputs to SNOMAP and ICEMAP are MODIS calibrated, geolocated surface reflectances and the MODIS cloud mask. The surface reflectance product is scheduled to be available by the third quarter of 1998, assuming that the launch occurs during the second quarter of 1998. In addition, an ancillary land/water mask will be required for SNOMAP. Current plans call for usage of the 1-km land/water

mask being generated by the EROS Data Center in Sioux Falls, SD.

Both SNOMAP and ICEMAP are coded in sensor-specific versions for prototyping. Specific sensor versions of the algorithms are necessitated by the fact that no current instrument has all the MODIS bands or capabilities. Current instruments have band coverage over some of the regions of the electromagnetic spectrum that MODIS will cover; these are used for developing algorithm concepts. The Landsat TM and the MAS are the sensors most relevant for testing algorithms before launch and for laying the foundation for the at-launch algorithms. However, TM views only $\pm 8^\circ$ from nadir and has only 7 spectral bands. The MAS views $\pm 43^\circ$ from nadir which is close to the MODIS view angles that will be used in our algorithm ($\pm 45^\circ$) and the MAS has 50 channels.

2.0 BACKGROUND

2.1 Remote Sensing of Snow Cover

Satellites are well suited to the measurement of snow cover because the high albedo of snow presents a good contrast with most other natural surfaces except clouds. Because of this characteristic, snow was observed in the first image obtained from the TIROS-1 weather satellite following its April 1960 launch (Singer and Popham, 1963). However, it was in the mid-1960s that snow was successfully mapped from space on a weekly basis following the launch of the ESSA-3 satellite. ESSA-3 carried the Advanced Vidicon Camera System (AVCS) that operated in the spectral range of $0.5 - 0.75 \mu\text{m}$ with a spatial resolution at nadir of 3.7 km. Using a variety of sensors, including the Scanning Radiometer (SR), Very High Resolution Radiometer (VHRR) and AVHRR sensors, snow cover has been mapped in the Northern Hemisphere on a weekly basis since 1966 by NOAA (Matson et al., 1986; Matson, 1991).

The average maximum snow cover in the Northern Hemisphere occurs in the month of February and is 46.2 million km^2 , based on 22 years of NOAA/NESDIS data. Work by Robinson et al. (1993) has shown that mean monthly snow cover in the Northern Hemisphere may have standard deviations of up to about $3 \times 10^6 \text{ km}^2$, and on an annual average the standard deviation is about $1.1 \times 10^6 \text{ km}^2$. Their work also shows that the standard error for monthly snow cover for the Northern Hemisphere can range from about 4 percent to about 25 percent of the monthly mean. (There is a definite seasonality in the deviations, with the greatest deviations observed for summer months and the least observed for winter months.)

Regional snow products, with 1-km resolution, are produced operationally in 3000 - 4000 drainage basins in North

America by the National Weather Service using NOAA National Operational Hydrologic Remote Sensing Center (NOHRSC) data (Carroll, 1990 and Rango, 1993). Passive-microwave sensors on-board the Nimbus 5, 6, and 7 satellites and the Defense Meteorological Satellite Program (DMSP) have been used successfully for measuring snow extent at a 25- to 30-km resolution through cloudcover and darkness since 1978 (Chang et al., 1987). Passive-microwave sensors also provide information on global snow depth (Foster et al., 1984). The NOAA/AVHRR and the DMSP Special Sensor Microwave Imager (SSM/I) are currently in operation. The Landsat Multispectral Scanner (MSS) and TM sensors, with 80-m and 30-m resolution, respectively, are useful for measurement of snow-covered area over drainage basins (Rango and Martinec, 1982). Additionally, Landsat TM data are useful for the quantitative measurement of snow reflectance (Dozier et al., 1981; Dozier, 1984 and 1989; Hall et al., 1989; Winther, 1992).

Reflectance of fresh snow is very high in the visible part of the electromagnetic spectrum, but decreases in the near-IR especially as grain size increases (O'Brien and Munis, 1975; Choudhury and Chang, 1981; Warren and Wiscombe, 1980; Warren, 1982). In addition, soot from industrial pollution becomes incorporated into the snowpack and this may decrease albedo and enhance snowmelt (Clarke and Noone, 1985; Warren and Clarke, 1985; Conway et al., 1996). Both because of natural aging and other factors (e.g. soot or volcanic ash deposition), the reflectance of snow decreases over time. Fresh snow can have a reflectance (integrated over the reflective part of the spectrum) up to about 80 percent but its reflectance may decrease to below 40 percent after snow crystals metamorphose.

Snow, like all natural surfaces, is an anisotropic reflector (Salomonson and Marlatt, 1968; Dirmhirn and Eaton, 1975; Steffen, 1987). The reflectance from snow is greatest in the forward direction and is largely specular. While freshly fallen snow can be nearly a Lambertian reflecting surface, as snow metamorphoses the specular component characteristic of forward scattering increases (Dirmhirn and Eaton 1975; Steffen, 1987).

2.2 Remote Sensing of Ice on Large Inland Lakes

The formation of lake ice brings shipping and transportation on inland waterways to a standstill for several months every year in many northern areas. In addition to the impact on humans, the presence or absence of ice on lakes can have a major influence on the ecology of a region. The presence of ice can govern the viability of fish life in a lake, for example.

Lake ice formation, thickness and break-up are also key indicators of regional climate especially in data-sparse regions which characterize much of the Arctic (Palecki and Barry, 1986). Lakes that freeze each winter are good indicators of regional climate change if key parameters such as the dates of freeze-up and break-up date and maximum ice thickness are measured over a decade-scale time frame.

Some northern regions have experienced climate warming over the past few decades (or longer) as measured in the permafrost record and in meteorological records (Chapman and Walsh, 1993). Schindler et al. (1990) showed that air and lake temperatures in the Experimental Lakes Area of northwestern Ontario have increased by 2°C, and the length of the ice-free season has increased by 3 weeks, according to 20 years of observations.

NOAA data have been used successfully to study lake ice on the Great Lakes. Because of the daily coverage of the NOAA satellites, data may be used operationally in spite of the fact that cloudcover obscures the surface for much of the time. Ice conditions are also of interest because open water areas or large leads in the Great Lakes, for example, contribute moisture to feed major snow storms. Much recent work on the remote sensing of the Great Lakes has been accomplished (see Assel et al., 1994).

2.3 Remote Sensing of Sea Ice Cover

Sea ice is an important component in the global climate system. Typically overlying approximately 7 percent of the world's oceans, sea ice experiences considerable seasonal variability in both hemispheres. In the Northern Hemisphere, the total extent of sea ice varies from a minimum of about 7.8×10^6 km² in September to a maximum of about 14.8×10^6 km² in March, and in the Southern Hemisphere the extent varies from about 4×10^6 km² in February to about 20×10^6 km² in September (Parkinson et al., 1987). Sea ice significantly reduces the amount of solar radiation absorbed at the Earth's surface, greatly restricts exchanges of heat, mass, and momentum between ocean and atmosphere, and affects the density structure of the upper ocean through the salt and heat fluxes associated with the freezing and melting processes. The changes in density structure at times lead to deep-water and even bottom-water formation, and the net equatorward advection of sea ice provides a transport of cold, low-salinity water out of the polar regions (Parkinson et al., 1987).

Satellite remote sensing is a useful tool for mapping sea ice edges and ice concentration globally. A global year-'round record of ice-covered Antarctic and Arctic seas was acquired from the Electrically Scanning Multichannel Microwave Radiometer (ESMR) on Nimbus-5 following its 1972 launch

(Zwally et al., 1983; Parkinson et al., 1987). Global maps of sea ice extent and concentration have been produced. The ability of passive-microwave instruments to collect data through cloudcover and polar darkness makes them well suited for global monitoring of sea ice, but microwave instruments do not collect data on albedo or thermal-emitted energy from sea ice. Information on albedo and temperature is important during the spring-summer-autumn seasons to help analyze energy exchange of sea ice. Measurement of sea ice albedo and temperature are possible with optical sensors such as the AVHRR and Landsat TM (Lindsay and Rothrock, 1993; Key and Haefliger, 1992 and Key and Collins, in press) and will be possible with MODIS.

There is no ideal sensor for the comprehensive study of sea ice. Nor does a single sensor exist that is capable of measuring or monitoring the many characteristics of sea ice thought to be important to climate modeling and global change. Combinations of sensors must therefore be employed (Comiso et al., 1991). The passive-microwave satellite data from the DMSP/SSM/I are obtainable daily through cloudcover and are useful for determination of ice type and concentration. The resolution of these data, which varies from about 15-30 km, is too poor for detailed studies of ice movement and lead structure. The imaging sensors on-board the Landsat and NOAA satellites are useful for ice movement and lead orientation studies, but all-too-frequently cloudcover intervenes to reduce the utility of the acquired data. Synthetic Aperture Radar (SAR) data are unsurpassed among remote sensors for showing lead orientation, shear zones and drift patterns throughout the year, day or night. The ERS-1 and JERS-1 satellites with SARs on-board have already provided much additional important information about sea ice since the 1991 launch of ERS-1. ERS-2 and RADARSAT data are also beginning to provide both local and regional coverage of sea ice. However, SARs do not provide global coverage on a daily basis as is possible with passive-microwave, NOAA and future MODIS sensors.

As it ages, newly-formed, smooth and thin sea ice is metamorphosed by temperature fluctuations, compressive and shear forces, surface currents and winds. In addition, the ice thickens and snow falls on top of the ice. Ridge formation and surface roughness increase with age, and the angular edges and smooth surfaces of first-year ice floes are transformed into rounded edges with hummocky, ridges and surfaces.

Because the amount of heat exchange between the ocean and the atmosphere is influenced by the thickness of sea ice, it is important to be able to distinguish first-year and multi-year sea ice using satellite data. The surface temperature of first-year and multi-year sea ice is different during the winter until the first-year ice attains a certain thickness;

these temperature differences, measured by AVHRR and future MODIS sensors, should aid in the determination of ice type.

Key and Haeffliger (1992) have shown that AVHRR thermal-IR data over snow-covered sea ice can be used to measure ice surface temperature under clear-sky conditions. An important potential error in IST measurement occurs when ice crystal haze forms over the ice surface. Ice crystal haze can result in ice surface temperature errors of approximately 2° K. Research has shown that the IST retrieval algorithm of Key and Haeffliger (1992) and Key and Collins (in press) is reliable in the Arctic, and is accurate to 0.3 - 2.1° K.

Much additional relevant research has been conducted. Only a cursory background is given in this report. Additional relevant literature is available in many sources, including Rango (1993) for snow studies, and Barry (1986) and Carsey et al. (1992) for sea ice studies.

3.0 MODIS INSTRUMENT CHARACTERISTICS

MODIS bands covering from the visible through the IR parts of the spectrum (Salomonson and Toll, 1991) will be used in the MODIS snow- and sea ice-mapping algorithms. Based on theoretical considerations and SNOMAP prototyping efforts, MODIS bands 4, 6, 7, 13, 16, 20, 26, 31, and 32 (Table 1) may be used as inputs. TM and AVHRR bands corresponding to MODIS bands are also listed in Table 1 for comparison. MODIS has higher spectral resolution than the TM and AVHRR sensors. MODIS band selection for SNOMAP has been largely determined by research done with comparable wavelength data from the TM sensors. As MODIS Airborne Simulator (MAS) data are analyzed, selection of optimum MODIS bands to use in SNOMAP and ICEMAP may to change.

Table 1. MODIS band centers and corresponding TM and AVHRR bands. The asterisks indicate that the MODIS band may be used as input to SNOMAP and/or ICEMAP.

MODIS band	Center Wavelength	Spatial Res. (m)	TM band	AVHRR band
---------------	----------------------	---------------------	---------	------------

1	0.645	250		1
2	0.858	250	4	2
3	0.469	500	1	
4*	0.555	500	2	
5	1.240			
6*	1.640	500	5	
7*	2.130	500	7	
8	0.412	1000		
9	0.443	1000		
10	0.488	1000		
11	0.531	1000		
12	0.551	1000		
13	0.667	1000	3	1
14	0.678	1000	3	1
15	0.748	1000		2
16*	0.869	1000	4	2
17	0.905	1000		2
18	0.936	1000		2
19	0.940	1000		2
20*	3.750	1000		3
21	3.959	1000		2
22	3.959	1000		
23	4.050	1000		
24	4.465	1000		
25	4.515	1000		
26*	1.375	1000		
27	6.715	1000		
28	7.325	1000		
29	8.550	1000		
30	9.730	1000		
31*	11.030	1000	6	4/5
32*	12.020	1000		5
33	13.335	1000		
34	13.635	1000		
35	13.935	1000		
36	14.235	1000		

Some snow/cloud discrimination may be accomplished with MODIS bands 6 and 7 located in the short-wave IR part of the spectrum. Further cloud-masking capabilities will be provided by the MODIS cloud-masking product.

Snow typically has very high visible reflectance (Figure 3). The specifications of MODIS band response ranges are great enough that MODIS visible sensors should not saturate when observing snow. (Conversely, sensor saturation over snow in TM bands 1-3 is common; saturation in TM band 4 is less common, but may occur after a new snowfall especially in spring. Sensor saturation over snow does not occur in TM bands 5 and 7). Based on the MODIS specifications, MODIS band 4 should not saturate if snow is present; it is thus an important band for snow identification and measurement.

The wide swath ($\pm 55^\circ$) of the MODIS sensor will be suitable for large-area coverage. Only data from $\pm 45^\circ$ view angles will be used for production of the snow maps because the distortions in pixel geometry and the increases in snow anisotropy at angles greater than 45° are likely to adversely affect our ability to calculate snow-covered area using SNOMAP. (Furthermore, as snow is an anisotropic reflecting surface, snow may not be mapped at non-nadir angles exactly as it is at nadir because SNOMAP was designed using the TM, which is a near-nadir-viewing sensor. This is currently being investigated using MAS data that just recently became available.) [See section 4.2.3.3.]

4.0 ALGORITHM DESCRIPTIONS

4.1 Philosophy Behind Selection of Algorithms

Many different algorithms for mapping snow have been studied. A band ratio, threshold-based algorithm was selected for the following reasons:

- 1) Its accuracy has been tested over a variety of surface covers relative to other derived snow-cover maps.
- 2) It runs automatically, without human intervention.
- 3) It is computationally frugal.
- 4) It can be employed globally.
- 5) It is straightforward computationally, and thus easy for the user to understand exactly how the product is generated.

While other algorithms may have greater accuracy at the regional and local scales, they do not fulfill the requirements relative to computer usage, automation and ability to map snow and ice globally.

The current version of SNOMAP has provide good results on TM images of a forested Minnesota landscape, northern Montana forests and prairie, the Sierra Nevada Mountains, in California, Chugach Mountains, an alpine environment in Alaska, Vatnajokull, ice cap, Iceland, and the Brooks Range, Alaska and others. ICEMAP has successfully mapped sea ice on the southwest coast of Greenland and in a scene of sea ice near Antarctica.

Snow has strong visible reflectance and strong short-wave IR absorbing characteristics. The Normalized Difference Snow Index (NDSI) is an effective way to distinguish snow from many other surface features. Both sunlit and some shadowed snow is mapped effectively. A similar index for vegetation, the Normalized Difference Vegetation Index (NDVI) has been

proven to be effective for monitoring global vegetation conditions throughout the year (Tucker, 1979 and 1986).

Other promising techniques, such as traditional supervised-multispectral classifications, spectral-mixture modeling, or neural-network analyses have not been shown to be usable for automatic application at the global scale. They are also computationally intensive. Training or interaction of an interpreter are required for successful application of techniques such as neural-network analysis. These techniques may progress to regional applications and possibly even global application in future years, but this evolution will not occur before 1997, when an at-launch algorithm is required to be delivered. However, in the post-launch time frame, if neural-network and/or spectral-mixture or other analysis techniques can be used to 'train' on the entire globe using MODIS data, then one of these methods might be implemented to map global snow and ice cover. If proven to improve the accuracy of the global snow-and ice-cover maps significantly, MODIS data will be reprocessed using a more advanced classification technique if the computational efficiency of the computer hardware has evolved enough to handle the increased load.

4.2 SNOMAP

The snow-mapping algorithm, SNOMAP (Hall et al., 1995; Riggs et al., 1996), is designed to identify whether snow is present in each 500-m pixel for each orbit. A global, daily snow product will be produced. A 10-day composited snow-cover product will be generated by compositing successive days of snow-cover products. This will yield maximum snow extent for the 10-day period. If a pixel were snow covered on any orbit during that period, then that pixel will be mapped as snow covered even if it were snow-free on all of the other orbits during the 10-day period. Other coverage and persistence statistics will also be included to assist analysis of the data product. Summary statistics and quality assurance (QA) data will be included as metadata.

There has been much discussion concerning the optimum compositing period for the snow and ice maps (e.g. see Hall, 1995). While weekly composites would correspond with the NOAA/NESDIS maps and the NOHRSC maps, some modelers are interested in longer compositing periods, e.g., 10 days to one month. Since the Science Working Group for the A.M. Project (SWAMP) suggested 10-day compositing periods, and since there appear to be no compelling reasons why another compositing period should be used, we decided to produce 10-day composites. This enables the snow and ice maps to be comparable with other derived products from MODIS, as well as products from other sensors. If a researcher wants to produce a composited product for any period other than a 10-

day period, from our daily product, this can be done using the daily data.

4.2.1 Normalized Difference Snow Index (NDSI)

The NDSI is useful for the identification of snow and ice, and for separating snow/ice and most cumulus clouds, to improve our ability to identify snow/ice and decrease reliance on single-band, "universal" thresholds. Figure 4 is a TM color composite of northern Montana, including Glacier National Park. Results of the SNOMAP algorithm, as applied to this scene are shown in Figure 5. The NDSI is a measure of the relative magnitude of the characteristic reflectance difference between the visible and short-wave IR reflectance of snow. The NDSI is insensitive to a wide range of illumination conditions, is partially normalized for atmospheric effects, and does not depend on reflectance in a single band. The NDSI is analogous to the normalized-difference vegetation index (NDVI) (Tucker, 1979 and 1986; Townshend and Tucker, 1984). Various other techniques employing ratioing techniques have been used previously to map snow, as discussed in section 1.0. For Landsat TM data the NDSI is calculated as:

$$\text{NDSI} = (\text{TM Band 2} - \text{TM Band 5}) / (\text{TM Band 2} + \text{TM Band 5}) \quad [1]$$

Pixels that are 50-60 percent or greater covered by snow have been found to have NDSI values \geq approximately 0.4 in our testing of a TM scene of the Sierra Nevada, California. Separation of snow and water is done by a TM band 4 reflectance test. If the reflectance of TM band 4 > 11 percent, and the NDSI ≥ 0.40 , snow covers 50 - 60 percent or more of the pixel. The NDSI threshold has been determined from detailed analysis of numerous TM scenes, comparisons with supervised-classification techniques and comparisons of a SNOMAP-derived map of the 10 May 1992 TM scene of the Sierra Nevadas with a snow map derived from Rosenthal and Dozier (1996).

Pure snow has a high NDSI but NDSI decreases as other features are mixed in a pixel. Snow in mixed pixels has an NDSI that is less than that for pure snow. An example of this can be seen in Figure 6, showing snow, snow in forest, and pure forest samples from TM data covering Glacier National Park, Montana. Pure snow can be distinguished by its high NDSI value. Samples obtained from dense forests from the same location in Glacier National Park were extracted from a late-summer TM scene (3 September 1990) and from a late-winter TM scene (14 March 1991), and are labeled 'forest summer' and 'forest winter,' respectively in **Figure 6**. The effect of snow cover on the NDSI of forest is evident in these samples.

4.2.2 Use of reflectances for Calculation of NDSI in the Prototype Algorithms

In the prototype SNOMAP algorithm, which employs TM data, at-satellite reflectance, r , is calculated as shown below (Markham and Barker, 1986):

$$r = (\pi L \lambda d^2) / (ESUN \lambda \cos \theta_s) \quad [2]$$

where;

$L \lambda$ is calibrated radiance

d is Earth-Sun distance

$ESUN \lambda$ is mean solar exoatmospheric irradiance

θ_s is SZA

The Earth-Sun distance and $ESUN$ can be obtained from a look-up table. For prototype efforts, we are assuming the Earth-Sun distance to be constant at 1.0 Astronomical Unit. For the prototype algorithm, the SZA of the TM scene center is used for each pixel. The operational MODIS algorithms will omit this step because MODIS reflectance product will be the input.

Equation 2 assumes that the surface being measured has isotropic reflectance properties even though this is not the case for snow, and other natural features. Thus, errors in calculation of reflectance due to the anisotropy of snow and ice may result. Such errors will likely be greater at larger angles off nadir. Also, as snow ages, its anisotropy increases. Additionally, errors in precise reflectance value due to anisotropy related to topographic variability will be inherent in the data (see section 4.2.3.3).

4.2.3 Estimate of Global Errors in Snow Mapping with SNOMAP

It is recognized that SNOMAP will perform better in some land covers than in others. Specifically, in tundra and prairie areas, and over large lakes, the errors in snow mapping will be very low. Results using the SNOMAP algorithm with TM and MAS data over these areas show 100 percent snow cover was mapped when they were known by field measurements to be 100 percent snow covered. In forested areas, errors may be much larger.

Using existing and future data from focused field and aircraft missions, we will develop an estimate of the errors inherent in using SNOMAP in different land covers, for example: agricultural (e.g. in the upper midwest of the U.S.), alpine (e.g. Glacier National Park, Montana), forest (e.g. the Boreal Forest in Saskatchewan), prairie (e.g. the Great Plains in eastern Montana) and tundra (e.g. the North Slope of Alaska). We will then be able to extrapolate the errors on a global basis, to gain a rough, but improved

understanding of global-scale errors to be expected in using SNOMAP.

Specifically, to determine global-scale error, the error calculated for each land cover will be weighted based on the percentage of the snow-covered Earth covered by each of the land-cover types. These land covers were selected because they cover a wide range of conditions encountered in snow-covered parts of the Earth.

Errors will be determined in different land covers by quantitative comparison of results of SNOMAP with snow maps derived through high-resolution aerial photography and field measurements. Data sets in alpine (see section 5.1.1.1), forested (section 5.1.1.2) and tundra (section 5.1.1.3) areas have already been acquired.

In the pre-launch time period, two methods will be tested for global error analysis. 1) The 1-km IGBP digital land-cover map of North America will be used to identify the five cover types discussed above (there are 17 land covers in the IGBP map). SNOMAP errors derived from each of the land covers from aircraft experiments will be extrapolated to the continental scale. 2) Using albedos derived by Robinson and Kukla (1985) from DMSP satellite data, Foster et al. (1994) were able to estimate forest-cover fraction, globally, and use this information to improve the results of an algorithm developed to map snow using passive-microwave data. They used derived forest-cover fraction to adjust an algorithm designed to calculate global snow-water equivalent from SSMI data, resulting in improvement of the results of the algorithm.

Initially, we will attempt to use this albedo-based classification to estimate expected errors in our SNOMAP results globally. In the future, we may also use the albedo categories, or some other method, to adjust the SNOMAP thresholds, to permit more snow to be mapped in forests, or other areas that prove to be contributing large errors to global snow mapping using SNOMAP.

4.2.3.1 Mapping snow in densely-forested areas

A significant limitation in mapping extent of snow cover is expected in situations of mixed pixels where snow cover is obscured by vegetation cover. Estimates of errors encountered in these situations will come from validation studies comparing SNOMAP-generated snow cover extent to other snow-cover data sets and/or ground observations (see section 4.2.3).

The snow-covered forested landscape is actually never completely snow covered because the tree branches, trunks and canopies often do not get or stay snow covered. Often, in

boreal forests, snow that falls on the coniferous tree canopy will not stay on the canopy for the entire winter due to sublimation. Thus, even in a continuously snow-covered area, much of the forested landscape will not be snow covered. It may be very difficult, even with field measurements and high-resolution air photos, to determine what percentage of the area is snow covered. Additionally, when viewing at off-nadir angles such as the $\pm 45^\circ$ angles that we plan to use with the MODIS sensor, the tree branches, canopies, etc., will obscure even more of the snow than when viewing at near-nadir angles (see section 4.2.3.3).

Much of the Earth's land surface is covered by dense forests. The boreal forest, the forest that stretches across the northern part of North America and Eurasia, is a prime example. Snow accumulates to greater depths and melts later in the spring in the boreal forests than in adjacent tundra or prairie areas (Foster et al., 1991). Though the boreal forests are always snow covered in the winter, within dense forests, snow that falls onto the ground through the canopy may not be visible from above. Some snow stays in the tree canopy and may thus be visible, but the snow often does not stay in the canopy during the entire winter. Snow in trees often sublimates before falling to the ground. Even with passive-microwave sensors, wherein microwave emission is measured, snow under a tree canopy is often not detected (Hall et. al., 1982; Foster et. al., 1991).

Comparison of results from snow mapping using TM data, and forest-cover classification was undertaken as part of MODIS pre-launch validation activities and in connection with the Boreal Ecosystem Atmosphere Study (BOREAS). The southern BOREAS study area in southern Saskatchewan, including Prince Albert National Park, consists of mixed deciduous and coniferous trees and stands consisting of predominately deciduous or coniferous trees. Several lakes are located in the test site. A 6 February TM scene and two MAS scenes, acquired on 8 February 1994, were acquired over Prince Albert National Park and the surrounding area in 1994. A TM scene of the same area, acquired on 18 January 1993, was also acquired. Field measurements and/or meteorological data show that the southern BOREAS study area was snow covered at the time of both Landsat overpasses. The only non-snow-covered areas were the tree trunks, stems and canopies.

The TM and MAS data were both registered to a forest-cover map developed using 6 August 1990 TM imagery of the BOREAS study area by Forrest Hall at NASA/GSFC (Hall et al., in press). Registration of the forest-cover map to the SNOMAP image derived from the 6 February 1994 TM scene enabled us to ascertain, quantitatively, the influence of different types of vegetation on snow mapping in this mixed forest. Throughout the 6 February 1994 TM scene, more snow was mapped

by SNOMAP in coniferous forests than in deciduous forests. Figure 7 shows a 512 X 512-pixel area within the full TM scene, from the forest-cover map and from the 6 February 1994 scene. In the areas classified as 'wet conifer,' substantially more snow is mapped than in adjacent areas of 'deciduous' trees. Only 14.4 percent of the snow was mapped in deciduous forests, though snow cover was otherwise continuous. In the coniferous forests, 72.1 percent of the snow was mapped. Note in Figure 7 that the boundary between the wet conifers and the deciduous forests (see arrow) is sharp and this boundary is clearly depicted in the SNOMAP image, Figure 7. This pattern prevails throughout the 6 February 1994 TM scene.

The deciduous trees are very dense in this area and, even from a 30-m tower, it is difficult to see snow beneath a deciduous forest when looking at off-nadir angles. Even without leaves or needles, the bare trunks and branches obscure most of the snow cover below. The density of the coniferous forest is also very high. Measurements show that nearby deciduous canopies average about 79 percent canopy density while conifers average about 88 percent (BORIS, 1994). These measurements were acquired using a densiometer which looks up through the trees. It is also relevant to consider the understory and its influence on snow-cover mapping. The deciduous aspen stands are known to have a considerable shrub understory, while the coniferous stands have little understory (Jon Ranson, oral communication). However, the ability of the shrub understory to preclude snow mapping in the winter, when defoliated, is not at all clear.

The snow that was mapped on the 6 February 1994 scene in the coniferous forest was most likely snow that was visible through the tree canopy and not snow that was on the tree canopy. (Though there had been a total of 13.4 cm of precipitation in the form of snow during the 10 days prior to the Landsat overpass, only a small amount of snow was visible on the coniferous tree canopy during the field work.) Other researchers (Pomeroy and Dion, in press) show that intercepted snow on the tree canopy sublimates quickly.

SNOMAP was also run on the 18 January 1993 TM scene, yielding quite different results than were obtained for the 6 February 1994 scene. For a subscene in common between the two scenes, 76 percent of the 18 January subscene was mapped as snow covered, while only 43 percent of the comparable part of the 6 February 1994 subscene was mapped as snow covered. And there is no apparent correspondence between forest-cover type and snow mapped on the 18 January 1993 scene the way there is on the 6 February 1994 scene.

Reasons for the differences in snow cover mapped by SNOMAP in the same area on the two scenes are unclear. One explanation

may be that on 18 January when the SZA was 78° , there is more transmission of light through both the deciduous and coniferous forests than there is on 6 February when the SZA was 74° . Greater SZAs are shown by John Pomeroy (oral communication, 1996) to increase light transmission into the canopy in this area. This would have the effect of illuminating the snow-covered ground more in January, permitting more snow to be mapped, relative to the February date. Though a 4° change in SZA seems unlikely to cause such a drastic change in light transmission, it may be that there is a critical threshold between 74° and 78° that, when reached, causes a dramatic change in light transmission through these forests. This should be explored further.

In conclusion, preliminary results using TM data show that the ability of the SNOMAP algorithm to map snow cover in forested areas is likely to be dependent on SZA and perhaps other factors. Much additional work on this is necessary in other forested areas (see section 5.1.1.4).

4.2.3.2 Snow/cloud discrimination

We will rely on the cloud-masking product, developed by Paul Menzel, Steve Ackerman and others at the University of Wisconsin, to map clouds and distinguish clouds and snow. Close coordination with that group will ensure a good result. For example, we are holding an aircraft and field experiment jointly with the University of Wisconsin cloud-masking group, in January and February 1997. Snow, lake ice and cloud masking is the focus of the experiment (see section 5.1.1.5.) The MAS will be the primary sensor on board.

For the prototype algorithms, snow/cloud-discrimination techniques are based on differences between cloud and snow/ice reflectance and emittance, (Figure 3). Clouds are highly variable and may be detected by their generally-high reflectance in the visible and near-IR parts of the electromagnetic spectrum (Rossow and Garder, 1993), whereas the reflectance of snow drops in the short-wave infrared part of the spectrum.

While the NDSI can separate snow from most obscuring clouds, it does not always identify or discriminate optically-thin cirrus clouds from snow. For this, MODIS channel 26, with the band center located at $1.375\text{ }\mu\text{m}$ will be used if necessary. At that wavelength, cirrus clouds are very strong absorbers, a property that may separate them from other features, including snow (Gao et al., 1993). Cirrus clouds may also be detected by brightness temperatures and differences in brightness temperature at 8.55, 11.0, and $12\text{ }\mu\text{m}$ (King et al., 1992). Channel 26 may be too sensitive to

the presence of optically-thin cirrus clouds and thus preclude snow-mapping through thin cirrus. Analyses of TM and MAS data show that SNOMAP can map snow under cirrus clouds at least some of the time. Investigation of the utility of channel 26 for use in SNOMAP and ICEMAP will not be feasible until the post-launch time frame because the 1.375 μm channel is not available on the MAS. Since this is primarily a cloud-masking task, we will work with the MODIS cloud-masking group to accomplish this.

4.2.3.3 Variation of Reflectance due to Sensor View Angle

Comparison of SNOMAP results derived from the Landsat satellite, with aircraft MAS-derived results has been undertaken. There is a marked difference in amount of snow mapped on the MAS and TM scenes covering the same area in the southern BOREAS test site when SNOMAP was used. Only 77 percent of the MAS scene was mapped as being snow covered, while 85 percent of a corresponding part of the TM scene was mapped as being snow covered. Field measurements showed that the entire area was snow covered except for some tree branches, stems and the tree canopies.

If we analyze individual strips of MAS and TM data, we find that there is generally a greater correspondence between amounts of snow mapped on MAS and TM at the near-nadir-view angles of the MAS than at the higher view angles of the MAS (Table 2). At higher viewing angles of the MAS ($> \pm 10^\circ$), less snow is mapped on the MAS scene than on the equivalent portions of the TM scene. (Percent snow mapped is not consistent on both sides of nadir because different land covers occur across the scenes thus affecting the amount of snow mapped.)

Table 2. Percent snow mapped and percent change in snow mapped relative to the TM, in individual strips of MAS and TM data, acquired on 8 and 6 February 1994, respectively. In all cases, more snow was mapped on the TM data than on the MAS data. R refers to the part of the images to the right of nadir and L refers to the part of the images to the left of nadir.

MAS View Angle	MAS	TM	percent change
$\pm 10^\circ$ off nadir	54.6	56.3	3.0
11-20°R	62.0	68.9	10.0
11-20°L	37.1	47.6	22.1
21-30°R	44.1	67.3	34.5
21-30°L	40.4	51.9	22.2

31-43°R	37.7	69.9	46.1
31-43°L	31.5	47.5	33.7

Within $\pm 10^\circ$ of nadir, both sensors map about the same percentage of snow cover (Table 2). Less snow is mapped by the MAS and TM at $11 - 20^\circ$ to left of nadir as compared to $11 - 20^\circ$ to the right of nadir, because there are dense deciduous tree stands to the left of nadir which effectively block some snow from being mapped. At the off-nadir view angles of the MAS, the tree canopies (both the defoliated stems from the deciduous trees, and the needles from the coniferous trees), may prevent much of the snow from being mapped by the MAS (and, in the future, from the MODIS). An additional effect may be the difference in SZA at the time of the MAS flight (SZA = 69°) versus at the time of the TM acquisition (SZA = 74°), allowing better light transmission to the canopy when the TM data were acquired as discussed above.

In order to determine, in a preliminary way, the effect of view angle on the snow reflectance measurements, since snow is known to be an anisotropic reflecting surface, we selected a snow-covered area on the North Slope of Alaska, imaged on 3 April 1995, by the MAS in its 50-channel configuration. This area was selected because it is flat and has very low vegetation; snow cover was continuous. Table 3 shows that the reflectance of MAS channel 1 ($0.54 \pm 0.044\mu\text{m}$) does not change very much from nadir to 43° . Reflectance in channel 1 is given as an example. Anisotropic reflectance properties of snow may therefore not be a large factor in contributing to the angular changes seen in Table 2. However, the position of the sensor with respect to the Sun is not taken into account here. Snow anisotropy is greater when looking toward the Sun. The main reason for the differences in amounts of snow mapped using TM and MAS data, as seen in Table 2, is the influence of the forests blocking the view of the snow on the ground at the off-nadir view angles of the MAS. More snow is obliterated from view at the off-nadir angles as compared to the near-nadir angles.

Table 3. Reflectance (in percent with standard deviation) of pixels from a 3 April 1995 MAS image acquired at approximately 68.8°N , 148.8°W on the North Slope of Alaska over snow-covered, non-forested terrain, from MAS channel 1 ($0.54 \pm 0.044\mu\text{m}$). R refers to the part of the area to the right of nadir, and L refers to the part of the area to the left of nadir.

Channel 1:

MAS View Angle	Reflectance	Standard Deviation
±10° off nadir	76.7	1.14
11-20°R	77.7	1.55
11-20°L	76.8	1.04
21-30°R	78.8	1.73
21-30°L	76.4	1.92
31-43°R	78.3	1.86
31-43°L	77.6	1.69

4.3 Lake Ice

The lake ice product will be produced along with, and as part of, the snow-cover product. Ice will be mapped in the following large inland water bodies: Lake Superior, Lake Michigan, Lake Erie, Lake Huron, Lake Ontario, Great Bear Lake, Great Slave Lake, Lake Winnipeg, Lake Athabaska, Lake of the Woods, Lake Sakami, Lake Nipigon and Reindeer Lake in North America; Lake Vanern, Lake Ladoga, Lake Baikal, Lake Peipus, Lake Balkhash and Onega Lake in Eurasia.

4.4 ICEMAP

4.4.1 Development of ICEMAP

ICEMAP is designed to identify whether sea ice is present in each 1-km pixel for each orbit and to calculate the IST. Daily and 10-day composited sea ice extent will be produced in the PGS. If sea ice is present in any pixel on any day during the 10-day compositing period, that pixel will be considered to be ice covered. ICEMAP is also designed to run automatically.

Land and clouds will be masked before ICEMAP is run. Criterion tests and decision rules for identifying sea ice may be modified versions of those used for SNOMAP. Identification of sea ice will also use surface temperature to assist in discrimination of ice cover and open water, especially if sea ice can be mapped at night by mapping temperature. If the IST algorithm proves to be accurate in detecting sea ice, it may be used in place of, or as part of, the ICEMAP algorithm to map sea ice day and night throughout the year.

4.4.2 Detection of Sea Ice

Measurements collected by researchers over the range of 0.4-2.4 μm show that the albedo of sea ice changes over the seasons (Grenfell and Perovich, 1984). Snow-covered sea ice

has albedo characteristics similar to snow, thus logic similar to that used to identify snow cover can be used to identify snow-covered sea ice.

As snow melts on sea ice, the albedo decreases across all wavelengths (Grenfell and Perovich, 1984). Open ocean typically has a very low albedo, in contrast to the more highly-reflective sea ice. Some types of sea ice, such as grease ice, however, may be difficult to identify with such criteria tests because they lack sharp contrast with open ocean.

Characteristics of areal extent, albedo, thickness of sea ice, ice margins, leads, ice types, motion and concentration, are important to observe (e.g. Barry, 1986). The primary contribution of the MODIS sea ice algorithm to the study and monitoring of sea ice will be the ability of MODIS data to provide some ice information at high spatial resolution (1 km) to augment the data provided by passive- and active-microwave sensors, and to map IST. Additionally, the ability to measure surface temperature in the winter, using MODIS data, should aid in the determination of ice type, and will be useful for estimating radiative and turbulent heat fluxes for large-scale climate studies.

The MODIS sea ice algorithm is being developed to identify sea ice by its reflectance characteristics in the visible and near IR and its sharp contrast to open water, and to map sea ice surface temperature. The darkness of polar winters will be a limiting factor in the use of visible channels. Cloud cover in the central Arctic Basin will be a limiting factor in mid-summer (Grenfell and Perovich, 1984) especially in the daily maps. Because the 10-day composite maps will be developed, it is expected that sea ice can be mapped during the spring, summer and autumn when the greatest changes are taking place in the extent and movement of sea ice. Winter sea ice mapping may be possible if the cloud-masking algorithm works well in polar darkness, and if the IST algorithm (see below) can readily separate ice and water.

4.4.3 Ice Surface Temperature (IST) Algorithm

IR bands (MODIS bands 31 and 32) will be used for mapping sea ice surface temperature. The surface temperature of open water is $> -1.8^{\circ}\text{C}$ while the surface temperature of saline ice $< -1.8^{\circ}\text{C}$ (271.2°K).

The basis of the MODIS IST algorithm is the work of Key and Collins (in press). Key and Collins (in press) state that the demonstrated accuracy of the algorithm is sufficient for most climate process studies. The major caveat with the algorithm is that it is applicable only to clear sky conditions; inadequate cloud masking may result in

significant error in estimating the IST. The heritage of the technique is Key and Haeffliger (1992) with substantiation of robustness and accuracy by later work (Key et al., 1994; Yu et al., 1995; Lindsay and Rothrock, 1994; Massom and Comiso, 1994).

Key and Haeffliger (1992) used the following equation to determine IST for snow-covered sea ice in the central Arctic under clear sky conditions.

$$IST = a + bT_{11} + cT_{12} + d[(T_{11} - T_{12})\sec\theta] \quad [3]$$

T_{11} -- brightness temperature °K in AVHRR band 4 (11 μ m)

T_{12} -- brightness temperature °K in AVHRR band 5 (12 μ m)

θ -- scan angle from nadir

a, b, c, d -- empirically-determined coefficients for atmospheric effects, notably humidity.

Key and Collins (in press) used the equation

$$IST = a + bT_{11} + c(T_{11} - T_{12}) + d[(T_{11} - T_{12})(\sec\theta - 1)] \quad [4]$$

where all variables are defined as in [3] except that the coefficients (a, b, c, d) are defined for temperature ranges of

$$\begin{aligned} T_{11} &< 240K \\ 240K &< T_{11} < 260K \\ T_{11} &> 260K. \end{aligned}$$

Equation [4] given by Key and Collins (in press) is reported by them to be superior to that of [3]. Linking the coefficients to temperature ranges also provides greater flexibility in application of the algorithm (Key and Collins, in press). Equation [4] is suitable for use with MODIS thermal data.

MODIS Level 1B data for the thermal emissive channels (31 and 32) will be generated and archived as radiance data. The radiance data can be converted to brightness temperature by inversion of Planck's equation.

Key et al. (1994) used an inversion of Plank's equation with an an emissivity term;

$$T = c_2v / \ln(1 + ((\epsilon c_1 v^3)/E)) \quad [5]$$

$$c_1 = 1.1910659 \times 10^{-5} \text{ mW m}^{-2} \text{ sr cm}^{-4}$$

$$c_2 = 1.438833 \text{ cm } ^\circ\text{K}$$

v = central wavelength cm^{-1}

E = radiance from sensor $\text{mW m}^{-2} \text{ sr cm}^{-4}$

T = $^\circ\text{K}$

ϵ = emissivity

Equation [4] can then be applied to determine IST.

4.4.4 Ice/Cloud Discrimination

The IST algorithm (Equation 4) is only valid for clear-sky conditions. Any cloud contamination may cause significant errors in calculation of IST. The MODIS cloud masking product will be utilized to identify clear sky conditions; pixels with a 95% or greater probability of being unobstructed by cloud. IST will be calculated only for those pixels. Other pixels will be identified as cloud contaminated.

Water vapor is the greatest atmospheric factor affecting the accuracy of the IST calculation under clear-sky conditions.

The primary difficulty with surface temperature retrieval when melt ponds and leads are present is the difference in emissivity between the open water and ice. The emissivity over water will be somewhat lower than that of snow or ice, say 0.96 compared to 0.99. This will make a difference of a few tenths of a degree (J. Key, written communication, 1996). The directional effects are also probably slightly different in melt ponds and leads as compared to snow- or ice-covered sea ice. There is likely to be more water vapor in the boundary layer when melt ponds and leads are present, but this is automatically handled by the algorithm. The coefficients are primarily used to correct for atmospheric water vapor.

Clouds pose many of the same problems in mapping sea ice as they do when mapping snow. Sea ice may move relatively rapidly and clouds may obscure this movement or make the movement of the sea ice appear incoherent when a 10-day time series, partially obscured by clouds, is compiled. Small ice floes, polynyas and leads at subpixel resolution contribute error to identification and mapping of sea ice. Global error analysis will be accomplished with other sources of data, e.g. passive-microwave and regional operational sea ice data products, to estimate error at regional and global scales in the post-launch time period.

4.4.5 Sources of Error

Sea ice identification does not have many of the complicating factors of varying surface covers that affect snow mapping, but there are complications that make sea ice mapping difficult. Because sea ice can vary in concentration from near zero to 100 percent, sea ice can give different reflectances and surface temperatures even within a scene, due to mixed-pixel effects. Sea ice can also have different reflectances depending on snow cover and the presence of

surface melt ponds. The presence of melt ponds and leads in the summer months will also affect the emissivity of the ice surface and therefore the calculation of ice surface temperature.

The accuracy of the IST is in the range of $0.3 - 2.1^{\circ}$ K (Key and Collins, in press). An expected accuracy for the MODIS IST product will be based on accuracies reported in Key and Haeffliger (1992), Lindsay and Rothrock (1994) and Key and Collins (in press), and on investigation with MODIS Airborne Simulator data which should allow us to define the expected accuracy for the MODIS IST.

Initially the coefficients of Key and Collins (in press) can be used in the MODIS IST algorithm. The coefficients may be modified based on validation studies, or by inclusion of a quantitative method to correct for atmospheric effects based on modeling of the atmosphere or quantitative measurements of water vapor from another sensor, or based on an Arctic climatology database.

Another method for customizing the coefficients to the MODIS sensor is to model snow-covered ice emissivity, MODIS sensor response, and the atmosphere to determine the estimated difference between the theoretical surface temperature, radiance measured by the sensor and the IST resulting from Equation [4]. The coefficients could be modified to allow agreement between the modeled and measured IST temperatures. Such methodology would follow the methods used by Key and Haeffliger (1992) and Key and Collins (in press).

MODIS Airborne Simulator (MAS) data are currently used to prototype the MODIS IST. Use of MAS data and associated field campaign data will be used to establish bounds for accuracy of MODIS IST, modification of coefficients, and other parameterizations of the algorithm and product generated. Since the MAS data from our April 1995 mission have only recently been received (delivery completed in October 1996), only very preliminary results are available.

4.5 Gridding of Snow-Cover and Sea Ice Cover Data Products

The snow and sea ice data products will be generated and gridded to a common grid. The snow and lake ice maps will be gridded in a sinusoidal projection common to the MODIS land group, at 500-m resolution. The sea ice maps will be re-gridded to a polar-stereographic map projection at 1-km resolution.

5.0 VALIDATION

5.1 Pre-Launch Validation Activities

5.1.1 Snow

5.1.1.1. Comparison with Sierra Nevada Snow Map derived from the 10 May 1992 TM Scene

Absolute accuracy can only be determined when SNOMAP results are compared to ground measurements, or air photos that have been validated by field measurements. There have been very few opportunities to do this so far. Thus far, our primary data used for validation is a carefully-mapped TM scene of the Sierra Nevada Mountains, California, acquired on 10 May 1992 and mapped using an independently-produced snow-mapping algorithm called Snow Covered Area (SCA) (Rosenthal, 1993; Rosenthal and Dozier, 1996). SCA is based on spectral mixture modeling. The SCA algorithm has been verified with low-altitude, high-resolution aerial photography and ground-based measurements, thus it provides a good test for SNOMAP.

The SNOMAP algorithm was run on the same Sierra Nevada scene, and results were compared with those of the SCA algorithm. SNOMAP compares extremely well to the results of SCA for pixels that are about 60% or more snow-covered. Agreement between the two techniques is >98%. NDSI also appears to be an excellent predictor of snow covered area for pixels that are moderately (30-60%) snow covered. For moderately snow-covered pixels, NDSI values map fractional snow cover with an accuracy of 80%.

SCA uses spectral mixture modeling to identify not only those pixels that are snow covered, but to estimate the fraction of each pixel that is covered with snow. This technique is based on the assumption that most pixels contain a mixture of surface materials, each with unique spectral properties. Several end member materials are chosen and a spectral model is created for each. For the Sierra Nevada TM scene, the end members are pure snow, rock and vegetation. All pixels are assumed to be some combination of these three end members.

A "learning sample" of several thousand pixels is selected in order to create a decision tree algorithm that will eventually classify the scene. The final decision tree algorithm is optimized, representing a balance between speed (simplicity) and accuracy in identifying snow. First, snow-free pixels are identified, using a band-ratioing technique similar to the NDSI, and masked, then the decision tree algorithm estimates the fraction of each remaining pixel covered by snow. The SCA algorithm assigns pixels containing snow to one of eight fractional snow cover categories: 96%, 84%, 72%, 60%, 50%, 38%, 22% and 9% snow-covered (Rosenthal and Dozier, 1996).

Following Rosenthal's (1993) work on spectral mixture modeling, the SNOMAP algorithm has been compared several times against the SCA model results. Visual inspection shows

that SNOMAP classifies fewer pixels as snow than does SCA. The total snow-covered area mapped by SNOMAP is 2.67 million km², compared with a total snow covered area of 2.97 million km² mapped by SCA, an agreement of 91%. A small number of pixels are mapped as snow by SNOMAP but not by SCA. However when SNOMAP is compared only with SCA snow cover categories about $\geq 60\%$, agreement is excellent (Figure 8).

Since the NDSI value is an important criterion for distinguishing snow-covered pixels from those that are not snow-covered, the NDSI values for the Sierra TM scene have been compared with their corresponding SCA snow cover classes. The SNOMAP algorithm produces data files of NDSI values and TM band 4 reflectances. These data were used to create a new image of the Sierra scene. First pixels with TM band 4 reflectance $\geq 11\%$ were masked. Then 3000 pixels from a mountainous part of the scene were selected from both the SCA and new NDSI images. From this group, non-snow pixels (those with SCA=0) were removed and the remaining 1483 snow-covered pixels were used for comparison (Figure 9).

Since there is some scatter in the data, particularly in the lower snow cover fractions, the mean NDSI values for each SCA category were calculated. These average values were then plotted, with error bars of two standard deviations from the mean (Figure 10). A linear regression was fitted to these data. The curve fit to the mean values rather than the whole data set reduces the influence of outlying data points. It is evident that NDSI is an excellent predictor of snow cover fraction.

Since there is benefit in defining snow-covered pixels that are about ≥ 60 percent snow covered, the NDSI data were grouped into three categories: 1-30%, 31-60% and 61-100% snow cover. The SCA data were grouped similarly (Figure 11). For the highest fractional snow cover category (61-100%) there is excellent agreement ($>98\%$) between the NDSI and SCA snow maps. At 31-60% snow cover, the agreement is 80%. For snow cover less than 30% the agreement is not good.

To further compare SNOMAP to the SCA algorithm, the original Sierra Nevada Landsat TM scene was spatially degraded to approximate the 500 x 500 m resolution of the MODIS snow cover product. Snow cover classification was undertaken using both SNOMAP and an updated version of the SCA algorithm on the spatially-degraded TM data, and classification results were compared to those achieved using the original resolution Landsat TM image.

Next, the DN values of the original Sierra Nevada Landsat TM Scene were spatially degraded to approximately the 500 x 500 m resolution of the MODIS snow cover product using a 17 x 17

pixel averaging window. The step size was equivalent to the size of the averaging window so that each original pixel was sampled only once. With an original TM pixel resolution of 28.5 m, the pixel dimensions of the simulated MODIS image were 485 x 485 m. The DN values of the both the degraded and original TM data were converted to at-satellite reflectance. SNOMAP and SCA algorithms were run using the reflectance values at both the degraded and original resolutions.

For consistency, the comparison of the two algorithms was done in a manner similar to that described in the preceding section. An updated version of the SCA algorithm is employed here and is the major source of discrepancy between the two comparisons. This version of the SCA algorithm used a decision tree trained on winter and spring scenes, and has more classes. In the following analysis, the original SCA classes were grouped into 10% snow cover classes (e.g. 0-9, 10-19, ...) to simplify the analysis.

Pixel size does not appear to greatly affect the performance of the SNOMAP algorithm. Consistent with the results derived using the full-resolution TM data, the agreement (defined as the percentage of pixels within a given SCA class that SNOMAP classifies as containing snow) between SNOMAP and SCA is very good for pixels containing > 50 % snow cover and poor for pixels containing < 50% snow as mapped by the SCA algorithm (Figure 12). For pixels with SCA values > 50%, the agreement between SNOMAP and SCA is 80% or greater for the TM degraded to MODIS pixel sizes. For < 50% SCA, the agreement between SNOMAP and SCA is poor with less than 20% agreement between the two methods. With the exception of the SCA class of 50-59%, the performance of SNOMAP was similar on both the original and degraded TM.

The reason for the discrepancy in classification accuracy as a function of SCA is quite clear. As can be seen in Figure 13, there is a natural grouping of the mean values of SCA classes by NDSI values. The 0.40 NDSI value presently selected as a threshold in SNOMAP falls in the natural break between these two groups which are composed of SCA classes above and below 50% snow cover, respectively. Based solely on these Sierra Nevada results, the present configuration of SNOMAP accurately classifies pixels containing snow cover if the snow covers ~50% or more of an individual MODIS pixel. The selection of 0.40 for a NDSI cutoff value seems appropriate. However, attempting to subdivide SCA into medium and low categories using the NDSI and Landsat band 4 presently employed in the SNOMAP algorithm appears less promising. No natural break seems to separate these lower snow cover classes.

5.1.1.2 BOREAS Experiment/February 1994

During February of 1994, in connection with the BOREAS project, the MODIS Airborne Simulator (MAS) was flown on the ER-2 aircraft over Prince Albert National Park, Saskatchewan, Canada. Simultaneous field measurements and lower-level aircraft flights were also acquired. Results of this work are described in Hall et al. (in press), and in sections 4.2.3.1 and 4.2.3.3 of this document.

5.1.1.3 April 1995 Alaska Experiment

In April 1995, the MAS on-board the ER-2 aircraft was deployed to image snow cover in Alaska and sea ice in the Bering Sea in conjunction with snow ground truth data collection. Also on-board was the Millimeter Wave Imaging Radiometer (MIR) instrument which acquires images in the microwave part of the spectrum. U.S. Army Cold Regions Research and Engineering (CRREL) and University of Alaska (Matthew Sturm and Carl Benson, respectively) scientists are collaborating on analysis of the field and aircraft measurements. Results from these flights should serve to aid in algorithm development and are important to help us to fine-tune the algorithm. The many spectral bands of the MAS, compared to the TM, will allow us to test new bands for possible inclusion in the algorithm.

Preliminary results of the MIR data are given in section 6.1. The calibrated MAS data were just recently received (last flight data received in October 1996). Therefore only very preliminary results have so far been obtained from this data set.

5.1.1.4 New England/Wisconsin Mission/January and February 1997

The next field and aircraft experiment is planned for a 3-week period in January and February 1997. The ER-2 with the MAS and the Millimeter Wave Imaging Radiometer (MIR), will fly in New England and Wisconsin in conjunction with the University of Wisconsin cloud-masking group and the Boston University land-cover group.

The main objectives of this mission are to improve snow/cloud discrimination, and to test the SNOMAP algorithm over areas of discontinuous snow cover, and to map lake ice and ice surface temperature. Most of the experiment will be run by the Wisconsin group, and one day will be devoted to our snow objectives in the New England area.

5.1.1.5 Validation of SNOMAP using supervised-classification techniques

Supervised classification was performed on 6 TM scenes (Table 4). The results of the supervised classification were then

compared with the results of the SNOMAP classification. The results of each classification were also compared with a band 5,4,2 color composite, digital reflectance image of each scene (Hall et al., 1995).

Table 4. Snow-covered area (SCA) in km² and percent of full TM scene determined using supervised versus SNOMAP classification techniques. GNP refers to Glacier National Park, Montana, Ch refers to a scene covering the Chugach Mts., Alaska, Vat refers to a scene covering Vatnajökull, Iceland and MN refers to a scene of northern Minnesota. Percent change refers to the difference in the amount of SCA mapped using the two different approaches for mapping snow cover.

	SCA (supervised)	SCA (SNOMAP)	% change
GNP 14Mar91	6,450 (19.1%)	10,631 (31.5%)	12.4
GNP 06Mar94	10,253 (30.3%)	10,953 (32.4%)	2.1
GNP 09May94	4,126 (12.2%)	4,006 (11.9%)	0.3
Ch 29Sep92	12,841 (38.0%)	16,021 (47.5%)	9.5
Vat 19Oct92	12,020 (35.6%)	13,033 (38.6%)	3.0
MN (09Mar85)	19,443 (57.6%)	21,534 (63.8%)	6.2

Detailed analysis of each scene indicated that the SNOMAP classification did a more consistent job than we could do when we performed the supervised classifications. While supervised versus SNOMAP results compared within about 6 percent, in 4 out of 6 cases, it is concluded that the SNOMAP classification is superior.

In the case of the 14 March 1991 Glacier National Park scene comparison, because of extensive cloud cover, the supervised classification was acknowledged to be poor. That is the reason for the large (12.4 percent) difference found when different classification techniques were used on that scene (Table 4). Using supervised classification, it was difficult to define pixels in cloud shadows that were snow pixels without inadvertently mapping non-snow pixels as well. In the case of the 29 September 1992 Chugach Mts. scene, a thick cirrus cloud in the northeastern part of the image was mapped as snow by SNOMAP, but not by us using the supervised technique. Whether SNOMAP is mapping the cloud or the snow underneath the cloud is unknown. The presence of this cloud caused the relatively large (9.5 percent) difference in snow-covered area classification results using the two classification techniques.

The SNOMAP classification filled in areas of shadowed snow much better than did the supervised classification, while in some cases (e.g. the Glacier National Park scene acquired on 9 May 1994), the supervised classification mapped more snow at the edges of snow-covered areas. Both classification techniques did a good job of mapping snow under very thin cirrus, while not mapping snow under thicker clouds. Both techniques mapped a few, stray, apparently non-snow pixels outside of the snow-covered areas. SNOMAP mapped more snow in dense forests (e.g. around Lake MacDonald on the 14 March 1994 Glacier National Park scene) than did the supervised-classification technique. Interestingly, SNOMAP did not map bare glacier ice as snow on a TM scene covering Vatnajökull ice cap, Iceland scene, while the supervised-classification technique did.

5.1.2 Sea Ice

5.2 Post-Launch Validation Activities

5.2.1 Snow

Focused field campaigns will be set up to do such validation. The first post-launch field and aircraft mission will be requested for February of 1998. Snow cover will be measured using field measurements and MAS underflights in the eastern and mid-western United States. Flights will be flown in various land covers: agricultural, alpine, forest and prairie. Field and low-level, high-resolution aircraft measurements will also be acquired. SNOMAP-derived errors in snow mapping in each of these categories will be determined.

5.2.1.2 Comparison with Other Global-Scale Products

SNOMAP results will be compared with other snow-cover maps and existing data sets of snow cover to determine relative error. The NOAA weekly snow charts and the NOHRSC regional data sets are good for comparison with SNOMAP results generated from MODIS. The data sets have an historical record and are generated operationally. SNOMAP results will also be compared with snow cover derived from Scanning Multichannel Microwave Imager (SSMI) data, if available, or Advanced Microwave Scanning Radiometer (AMSR) data after the launch of the first EOS-PM platform in 2000. Comparison of SNOMAP results with these independently-produced snow data sets will allow errors to be identified that will permit us to determine the accuracy of the global maps relative to one another.

NOAA plans to place an AVHRR, enhanced with a 1.6 μm channel for snow and cloud discrimination, on the NOAA K - N series of polar-orbiting platforms. NOAA-K will be ready for launch in the fall of 1996, but will not be launched until NOAA-12

fails. The 1.6 μm channel on NOAA-K will be available for testing, but not for regular use on NOAA-K. A change in the technique for the generation of NOAA snow and ice charts is expected with the launch of NOAA-L. At that time, a snow/cloud discrimination technique using the 1.6 μm channel will probably be implemented. The techniques used by NOAA and the snow and ice data sets they generate can then be used for validation for MODIS snow and cloud discrimination techniques employing the MODIS 1.6 μm band. NOAA experience for snow/cloud discrimination with satellite data at 1.6 μm will be drawn upon for refinement of SNOMAP in the near-launch time frame. We are working closely with the NOAA/NESDIS group so we can share ideas and algorithms for snow-cover mapping and validation.

5.2.2 Sea Ice

6.0 COMBINATION OF MODIS AND OTHER EOS DATA FOR SNOW- AND SEA ICE-COVER MAPPING

The combined use of visible, near-IR, short-wave IR and microwave sensors to map snow will lead to an ability to map snow extent, albedo and water equivalent, and sea ice concentration. Because passive-microwave sensors are generally unaffected by cloudcover over snow- and ice-covered areas, it will be advantageous, in the EOS era after the launch of the second EOS platform, to use MODIS data in conjunction with AMSR data to map snow extent and depth globally. Many of our pre-launch validation efforts deal with combining the optical and passive-microwave data. For example, our Alaska '95 mission had passive-microwave sensors as well as the MAS on board (Hall et al., 1996).

Passive-microwave data have been used to map Northern Hemisphere snow cover at a resolution of up to 30 km since 1978 even through darkness and cloudcover. The passive-microwave data also provide an estimate of snow-water equivalent in many areas. Parameters affecting the passive-microwave response of snow include: water equivalent, density, grain size, temperature, surface roughness, forest-cover fraction and forest type. Problems inherent in the interpretation of the data include: the coarse resolution is not suitable for most regional snow studies, in densely-forested areas algorithms underestimate snow-water equivalent, and derivation of snow-water equivalent is dependent upon snow and land-cover characteristics.

Similarly, passive-microwave data have been used to map sea ice extent and concentration. In the future, with AVHRR data from NOAA-K and beyond, and with MODIS data, optical data can be used to provide detail that passive-microwave data cannot, including IST, when conditions are clear. Used in synergy, optimum sea ice information will be possible.

6.1 Preliminary Analysis of Snow Cover in Alaska using Aircraft Microwave Data (April 1995)

From 31 March to 25 April, 1995, a mission was conducted to study snow cover in northern and central Alaska, respectively (Hall et al., 1996). The utility of high frequency passive-microwave aircraft data is assessed as is the influence of a variety of surface cover types on the microwave brightness temperatures of dry and melting snow. The aircraft data included the Millimeter-wave Imaging Radiometer (MIR) and the MODIS Airborne Simulator (MAS).

The MIR is a mechanically-scanned imaging microwave radiometer that measures radiation at the following frequencies: 89, 150, 183.3 ± 1 , 183.3 ± 3 , 183.3 ± 7 and 220 GHz. It has an angular resolution of about 3.5° . It is a cross-track scanner with an angular swath width of about 100° , centered at nadir. Its polarization vector is in the horizontal plane and perpendicular to the velocity vector of the aircraft so that the measured radiation is a mixture of vertical and horizontal polarizations depending on the viewing angles. The temperature sensitivity is ≤ 1 K for all channels. The MIR data in this study have a spatial resolution of approximately 1 km at nadir.

The ability to infer snowpack thickness using passive-microwave data has been recognized for many years. However, many factors have been found that complicate the relationship between passive microwave brightness temperature and snow depth (Chang et al., in press).

Field measurements of snow depth, density, grain size and shape were made in Fairbanks ($64^\circ 50'N$, $147^\circ 48'W$) and at Ester Dome which is about 5 km northwest of Fairbanks, as well as in other parts of Alaska. Aircraft flight lines were flown in a grid pattern in central Alaska, including Fairbanks, on 5, 6, 13 and 21 April. The MIR data have been gridded to a polar stereographic equal area map. In addition, a vegetation map of Alaska (Kuchler, 1985) was registered to the MIR data to compare with the aircraft data.

Field and air-temperature measurements showed that the snow in and near Fairbanks was melting during the daytime during the month of April. Except within the city, snow cover was nearly continuous. Table 5 shows snow depths from a location in Fairbanks and at Ester Dome. Table 6 shows air temperatures at the approximate time of the aircraft takeoff on the flight days over the 'Fairbanks grid.' Each flight over the Fairbanks grid lasted about 2 hours and 20 minutes.

Table 5. Snow depths in Fairbanks and at Ester Dome on selected dates in April.

<u>Date</u>	<u>Fairbanks</u>	<u>Ester Dome</u>
4/1/95	59 cm	---
4/2/95	54 cm	---
4/6/95	39 cm	---
4/7/95	35 cm	---
4/8/95	---	100 cm
4/11/95	23 cm	---

Table 6. Average air temperatures at approximate times of aircraft takeoffs, and time of flights over the 'Fairbanks grid.'

<u>Date</u>	<u>°C</u>	<u>Fairbanks local time</u>
4/5/95	8°	10:50 - 13:11
4/6/95	3°	8:42 - 11:01
4/13/95	10°	11:08 - 13:36
4/21/95	-1°	6:59 - 9:29

Snow in Fairbanks was actively melting during the daytime during the month of April. As soon as snow becomes wet, scattering is reduced as the crystals become coated with liquid water. As a result, the snowpack behaves as a lossy medium, and the brightness temperature increases. In the vicinity of Fairbanks, the 89-GHz brightness temperatures averaged 263 K, while in the southern part of the study area (central Alaska Range) brightness temperatures were ≈ 210 K on 5 April. Deeper snow and lower temperatures contributed to lower brightness temperatures there. Additionally, on lines flown north of Fairbanks, toward the Brooks Range and on the North Slope, also on 5 April, brightness temperatures are 10-40 K lower than in the Fairbanks area because the snow to the north was still dry in April (Figure 14). Also, in the Brooks Range and on the North Slope, there are no trees to increase the brightness temperatures there.

Comparison of the vegetation map with the MIR data shows that several land-cover types influence the microwave signal. On each of the 4 MIR images (at 89 GHz) for the Fairbanks grid, a boundary between the black spruce forest and the meadow dryas is evident at a latitude of approximately 64°N, just south of Fairbanks. Coniferous trees emit more microwave radiation than do tundra or dryas vegetation, and this is one explanation for the higher brightness temperatures in the black spruce forests.

In the central part of the Fairbanks grid, brightness temperatures are generally quite high due to the melting snow. The relatively high brightness temperatures there overwhelm the brightness-temperature differences that result from land-cover variability. This is especially true on April 13, when the air temperatures were the highest of the 4 flight days (Table 6), and presumably, when melting covered the largest extent of area.

Other regions of interest are where finger-like projections of the spruce-birch forest to the east of Fairbanks intersect dryas meadows and barren areas. Brightness temperatures are higher in the spruce-birch forest (≈ 261 K) than in the dryas meadows and barren areas (≈ 251 K) presumably due to the higher emissivity of the trees.

The land-cover type is shown to influence microwave brightness temperature under dry snow conditions. Snow-covered forests cause higher brightness temperatures than do snow-covered dryas meadows and tundra. However, when the snowpack is wet, the high emissivity of the snowpack overwhelms the contribution of the vegetation to the brightness temperature.

Work will continue on the current data set to investigate the influence of land cover particularly the influence of the dryas meadows and black spruce. Satellite data will be analyzed in conjunction with MIR data in order to modify snow depth retrieval algorithms so that they are more responsive to the snow and land surface conditions encountered in central and northern Alaska. In addition, analysis of MIR and MAS data, together, will be undertaken.

7.0 References

- Assel, R.A., T.E. Croley II and K. Schneider, 1994: Normal daily temperatures and ice cover of the Laurentian Great Lakes of North America, Abstract only, 51st Eastern Snow Conference, 15-16 June 1994, Dearborn, MI.
- Barry, R.G., 1986: The sea ice data base, In: The Geophysics of Sea Ice, Untersteiner, N. (ed.), Plenum Press, NY, pp.1099-1134.
- BORIS (BOREAS Information System), 1994: Canopy density summary by Robert E. Davis, BORIS/NASA/GSFC Greenbelt, MD.
- Bromwich, D.H., R.-Y. Tzeng and T.R. Parish, 1994: Simulation of the modern arctic climate by the NCAR CCM1, Journal of Climate, V.7, pp.1050-1069.
- Bunting, J.T. and R.P. d'Entremont, 1982: Improved cloud detection utilizing defense meteorological satellite program near infrared measurements, Air Force Geophysics Laboratory, Hanscom AFB, MA, AFGL-TR-82-0027, Environmental Research Papers, No. 765, 91 p.
- Carsey, F.D., 1992: Microwave Remote Sensing of Sea Ice, American Geophysical Union, Geophysical Monograph 68, 462 p.
- Carroll, T.R., 1990: Operational airborne and satellite snow cover products of the National Operational Hydrologic Remote Sensing Center, Proceedings of the forty-seventh annual Eastern Snow Conference, June 7-8, 1990, Bangor, Maine, CRREL Special Report 90-44.
- Chang, A.T.C., J.L. Foster and D.K. Hall, 1987: Microwave snow signatures (1.5 mm to 3 cm) over Alaska, Cold Regions Science and Technology, 13:153-160.
- Chang, A.T.C., J.L. Foster, D.K. Hall, B.E. Goodison, A.E. Walker, J.R. Metcalfe and A. Harby, in press: Snow parameters derived from microwave measurements during the BOREAS winter field campaign, submitted to Journal of Geophysical Research.
- Chapman, W.L. and J.E. Walsh, 1993: Recent variations of sea ice and air temperature in high latitudes, Bulletin of the American Meteorological Society, 74:33-47.
- Choudhury, B.J., and Chang, A.T.C., 1981: The albedo of snow for partially cloudy skies, Boundary Layer Meteorology, 20:371-389.

Clarke, A.D., and Noone, K.J., 1985: Soot in the Arctic snowpack: a cause for perturbations in radiative transfer. Atmospheric Environment, 19:2045-2053.

Comiso, J.C., Wadhams, P., Drabill, W.B., Swift, R.N., Crawford, J.P. and Tucker III, W.B., 1991: Top/bottom multisensor remote sensing of arctic sea ice. Journal of Geophysical Research, 96(C2):2693-2709.

Conway, H., A. Gades and C.F. Raymond, 1996: Albedo of dirty snow during conditions of melt, Water Resources Research, 32:1713-1718.

Dirmhirn, I., and Eaton, F.D., 1975: Some characteristics of the albedo of snow. Journal of Applied Meteorology, 14: 375-379.

Dozier, J., 1984: Snow reflectance from Landsat-4 thematic mapper. I.E.E.E. Transactions on Geoscience and Remote Sensing, 22:323-328.

Dozier, J., Schneider, S.R., and McGinnis, D.F., Jr. 1981: Effect of grain size and snowpack water equivalence on visible and near-infrared satellite observations of snow. Water Resources Research, 17:1213-1221.

Dozier, J. 1989. Spectral signature of alpine snow cover from the Landsat Thematic Mapper, Remote Sensing of Environment 28:9-22.

Foster, J.L., D.K. Hall, A.T.C. Chang and A. Rango, 1984: An overview of passive microwave snow research and results, Reviews of Geophysics, 22:195-208.

Foster, J.L., A.T.C. Chang, D.K. Hall and A. Rango, 1991: Derivation of snow water equivalent in boreal forests using microwave radiometry, Arctic, 44 (Supp. 1):147-152.

Foster, J.L. et al., 1994: Snow mass in boreal forests derived from a modified passive microwave algorithm, Multispectral and Microwave Sensing of Forestry, Hydrology, and Natural Resources, Mougin, E., K.J. Ranson and J.A. Smith (ed.), proceedings of the EROPT series, SPIE, 26-30 September 1994, Rome, Italy.

Gao, B.-C., A.F.H. Goetz and W.J. Wiscombe, 1993: Cirrus cloud detection from airborne imaging spectrometer data using the 1.38 mm water vapor band, Geophysical Research Letters, 20(4):301-304.

Grenfell, T.C. and D.K. Perovich, 1984: Spectral albedos of sea ice and incident solar irradiance in the southern

Beaufort Sea, Journal of Geophysical Research, 89(C3):3573-3580.

Hall, D.K., J.L. Foster and A.T.C. Chang, 1982: Measurement and modeling of microwave emission from forested snowfields in Michigan, Nordic Hydrology, 13:129-138.

Hall, D.K., A.T.C. Chang, J.L. Foster, C.S. Benson and W.M. Kovalick, 1989: Comparison of in-situ and Landsat-derived reflectance of Alaskan glaciers, Remote Sensing of Environment, 28:23-31.

Hall, D.K. (ed.), 1995: Proceedings of the First MODIS Snow and Ice Workshop, 15-17 September 1995, Greenbelt, MD, 128 p.

Hall, D.K., G.A. Riggs and V.V. Salomonson, 1995: Development of methods for mapping global snow cover using moderate resolution imaging spectroradiometer data, Remote Sensing of Environment, 54:127-140.

Hall, D.K., J.L. Foster, A.T.C. Chang, D.J. Cavalieri and J.R. Wang, 1996: Analysis of snow cover in Alaska using aircraft microwave data (April 1995), Proceedings of the IGARSS '96 Symposium, 27-31 May 1996, Lincoln, NE, 4:2246-2248.

Hall, D.K., J.L. Foster, A.T.C. Chang, K.S. Brown and G.A. Riggs, in press: Mapping snow cover through forests in the southern BOREAS test site in Saskatchewan, submitted to JGR.

Key, J. and M. Haeffliger, 1992: Arctic ice surface temperature retrieval from AVHRR thermal channels, Journal of Geophysical Research, 97:(D5):5885-5893.

Key, J., Maslanik, J.A., Papakyriakou, T., Serreze, M.C., and Schweiger, A.J. 1994. On the validation of satellite-derived sea ice surface temperature, Arctic, 47:280-287.

Key, J.R. and Collins, J.B., in press: High-latitude surface temperature estimates from thermal satellite data, Submitted to Remote Sensing of Environment, June 1996.

King, M.D., Kaufman, Y.K., Menzel, W.P., and Tanre, D., 1992: Remote sensing of cloud, aerosol, and water vapor properties from the moderate resolution imaging spectrometer (MODIS), IEEE Transactions on Geoscience and Remote Sensing, 30:2-27.

Kuchler, A.W., 1985: Potential Natural Vegetation, USGS Map from National Atlas, sheet no. 89.

Kyle, H.L., R.J. Curran, W.L. Barnes and D. Escoe, 1978: A cloud physics radiometer, Third Conference on Atmospheric Radiation, Davis, CA, pp.107-109.

Lindsay, R. and D. Rothrock, 1993: The calculation of surface temperature and albedo of Arctic sea ice from AVHRR, Annals of Glaciology, 17:391-397.

Lindsay, R.W., and Rothrock, D.A. 1994. Arctic sea ice temperature from AVHRR, Journal of Climate, 7:174-183

Liston, G.E., 1995: Local advection of momentum, heat, and moisture during the melt of patchy snow covers. Journal of Applied Meteorology, 34(7):1705-1715.

Markham, B.L., and J.L. Barker, 1986: Landsat MSS and TM post-calibration dynamic ranges, exoatmospheric reflectances and at-satellite temperatures, in EOSAT Technical Notes, No. 1, August, pp. 3-8.

Massom, R., and Comiso, J.C. 1994. The classification of Arctic sea ice types and the determination of surface temperature using advanced very high resolution radiometer data, Journal Geophysical Research, 99, C3:5201-5218.

Matson, M., C.F. Ropelewski and M.S. Varnadore, 1986: An atlas of satellite-derived northern hemisphere snow cover frequency, National Weather Service, Washington, D.C., 75 pp.

Matson, M., 1991: NOAA satellite snow cover data, Palaeogeography and Paleoecology, 90:213-218.

O'Brien, H.W., and Munis, R.H., 1975, Red and near-infrared spectral reflectance of snow. In: Operational Applications of Satellite Snowcover Observations, edited by A. Rango, NASA SP-391 (Washington, D.C.: NASA), pp. 345-360.

Palecki, M.A. and R.G. Barry, 1986: Freeze-up and break-up of lakes as an index of temperature changes during the transition seasons: a case study in Finland. Journal of Climate and Applied Meteorology, 25:893-902.

Parkinson, C.L., J.C. Comiso, H.J. Zwally, D.J. Cavalieri, P. Gloersen and W.J. Campbell, 1987: Arctic Sea Ice, 1973-1976: Satellite Passive-Microwave Observations, NASA SP-489, GPO, Washington, D.C.

Rango, A., 1993: Snow hydrology processes and remote sensing, Hydrological Processes, 7:121-138.

Rango, A. and J. Martinec, 1982: Snow accumulation derived from modified depletion curves of snow coverage, Symposium on

Hydrological Aspects of Alpine and High Mountain Areas, in Exeter, IAHS Publication No. 138, pp. 83-90.

Riggs, G.A., D.K. Hall and V.V. Salomonson, 1996: Recent progress in development of the Moderate Resolution Imaging Spectroradiometer snow cover algorithm and product, Proceedings of the IGARSS '96 Symposium, 27-31 May 1996, Lincoln, NE, 1:139-141.

Robinson, D.A., Dewey, K.F., and Heim, Jr. R.R., 1993: Global snow cover monitoring: an update. Bulletin of the American Meteorological Society, 74:1689-1696.

Rosenthal, W., 1993: Mapping montane snow cover at subpixel resolution from the Landsat thematic mapper, Univ. of California Santa Barbara M.A. thesis, 70 p.

Rossow, W.B. and Garder, L.C., 1993: Validation of ISCCP cloud detection, Journal of Climate (in press).

Salomonson, V.V., and Marlatt, D.C., 1968: Anisotropic solar reflectance over white sand, snow and stratus clouds. Journal of Applied Meteorology, 7:475-483.

Salomonson, V.V. and D.L. Toll, 1991: The moderate resolution imaging spectrometer-radar (MODIS-N) facility instrument, Advances in Space Research, 11:231-236.

Schindler, D.W., K.G. Beaty, E.J. Fee, D.R. Cruikshank, E.R. DeBruyn, D.L. Findlay, G.A. Linsey, J.A. Shearer, M.P. Stainton and M.A. Turner, 1990: Effects of climatic warming on lakes of the central boreal forest. Science, 250:967-970.

Singer, F.S. and R.W. Popham, 1963: Non-meteorological observations from weather satellites, Astronautics and Aerospace Engineering, 1(3):89-92.

Steffen, K., 1987, Bidirectional reflectance of snow. B.E. Goodison, R.G. Barry, and J. Dozier, (editors): Large scale effects of seasonal snow cover. Proceedings of the IAHS Symposium held in Vancouver on 19-22 August 1987 (Vancouver, Canada: IAHS), pp. 415-425.

Townshend, J. R.G., and C.J. Tucker, 1984: Objective assessment of Advanced Very High Resolution Radiometer data for land cover mapping, International Journal of Remote Sensing 5:497-504.

Tucker, C.J., 1979: Red and photographic infrared linear combinations for monitoring vegetation, Remote Sensing of Environment, 8:127-150.

Tucker, C.J., 1986: Maximum normalized difference vegetation index images for sub-Saharan Africa for 1983-1985, International Journal of Remote Sensing, 7:1383-1384.

Warren, S.G., 1982: Optical properties of snow. Reviews of Geophysics and Space Physics, 20:67-89.

Warren, S.G., and Clarke, A.D., 1985: Soot from Arctic haze: radiation effects on the Arctic snowpack. Snowwatch, World Data Center A for Glaciology (snow and ice) Report GD-18, edited by G. Kukla, R.G. Barry, A. Hecht and D. Wiesnet. Boulder, Colorado.

Warren, S.G., and Wiscombe, W.J., 1980: A model for the spectral albedo of snow II: snow containing atmospheric aerosols. Journal of the Atmospheric Sciences, 37:2734-2745.

Winther, J.-G., 1992: Landsat thematic mapper (TM) derived reflectance from a mountainous watershed during the snow melt season, Nordic Hydrology, 23:273-290.

Yu, Y. Rothrock, A., and Lindsay, R.W. 1995. Accuracy of sea ice temperature derived from the advanced very high resolution radiometer, Journal of Geophysical Research, 100, C3:4525-4532.

Zwally, H.J., J.C. Comiso, C.L. Parkinson, W.J. Campbell, F.D. Carsey and P. Gloersen, 1983: Antarctic Sea Ice, 1973-1976: Satellite Passive-Microwave Observations, NASA, SP-459, 206 p., G.P.O., Wash., D.C.

8.0 Figure Captions

1a. Processing flow of MODIS snow data products. Algorithm processes are depicted as circles. Data inputs are depicted as shaded rectangles with rounded corners; light gray inputs are used in Version 1 of the algorithms, dark gray inputs are expected to be used in a future version. Data products are depicted as light gray rectangles.

1b. Summary of analysis steps in SNOMAP for a granule of MODIS data. Data inputs are depicted as shaded rectangles; data inputs used in Version 1 are in light gray, data inputs for future versions are in dark gray.

2a. Processing flow of MODIS sea ice data products. Algorithm processes are depicted as circles. Data inputs are depicted as shaded rectangles with rounded corners; light gray inputs are used in Version 1 of the algorithms, dark gray inputs are expected to be used in a future version. Data products are depicted as light gray rectangles.

2b. Summary of analysis steps in ICEMAP for a granule of MODIS data, and major steps in ten day composite. Data inputs are depicted as shaded rectangles. Major processing steps are listed in the lined rectangles.

3. Spherical albedo of snow and clouds. (After King et al., 1992; O'Brien and Munis, 1975).

4. TM color composite (bands 5, 4 and 2) of northern Montana, including Glacier National Park (i.d.#5256917454).

5. Snow map derived from TM scene shown in Figure 4, using SNOMAP. SNOMAP identified 10,670 km² of snow in the scene. (Clouds were identified and masked by supervised classification to simulate the MODIS cloud mask.)

6. Histogram of snow and forest samples, and forest samples from 14 March 1991 and 03 September 1990 TM images, respectively, of Glacier National Park, Montana region. Snow sample from snow-covered surface of frozen Lake McDonald (n=2025) from the 14 March 1991 scene. Snowy forest (n=1375) sample from a snow-covered forest valley on the 14 March 1991 scene. Forest summer (n=2025) and winter (n=2025) samples from the same location in dense forest to the immediate west of Lake McDonald.

7. Comparison of a Landsat-derived land-cover classification by Forrest Hall, NASA/GSFC (using the 6 August 1990 TM image, id.#52349-17181100), of the BOREAS study area (image on left) with the SNOMAP classification (using the 6 February 1994 TM image, id.# 53629-171919) (image on right).

8. SNOMAP and SCA results for SCA categories 96, 84, 72 and 60. Pixels mapped as snow by both algorithms are shown in white. Pixels mapped as snow by SCA but not by SNOMAP are magenta. Pixels mapped as snow by SNOMAP but not by SCA are cyan. For these SCA categories, agreement between the two algorithms is >98%.

9. Plot of NDSI value and SCA snow cover category for 1483 snow-covered pixels in Sierra Nevada TM scene. SNOMAP threshold of NDSI=40 is indicated by the heavy dashed line. This better illustrates the results of the previous figure: all pixels in the 72%, 84% and 96% SCA categories have NDSI >40, and are thus mapped as snow by SNOMAP. Only half the pixels in the 60% snow cover category have NDSI >40, thus agreement between the two techniques is approximately 50%, and in the lower snow cover categories all pixels have NDSI <40, and are thus not mapped as snow by SNOMAP.

10. Plot of the mean NDSI value of each group of pixels from Figure 9 and SCA category. Average NDSI for each group is plotted as a filled circle with error bars of two standard deviations from the mean. A linear regression was fitted to this data, with an r^2 of 0.991. Thus for TM data, NDSI value appears to be an excellent predictor of snow cover fraction. This linear regression was used to calculate fractional snow cover for each pixel in the Sierra TM scene.

11. Snow cover fractions have been grouped into three categories: 1-30%, 31-60% and 61-100% snow covered. The results of the SCA and NDSI techniques are compared for these groupings. Agreement in the 61-100% category is excellent. In the 31-60% snow cover category the NDSI technique overestimates the number of snow-covered pixels by approximately 20%. In the 1-30% category the NDSI technique does a poor job of distinguishing snow from other types of ground surface.

12. Bar graph showing the agreement in snow cover classification between the SNOMAP and SCA algorithms as a function of the percentage of snow-covered area. Classes represent differing percent snow cover within a pixel as determined by the SCA algorithm. Agreement is defined as the percentage of pixels within a given snow cover class that SNOMAP classifies as containing snow. The gray bars indicate the agreement between the SNOMAP and SCA algorithms for the Sierra Nevada TM image at its original resolution. The black bars indicate the agreement for TM image spatially degraded to 500-m resolution.

13. Scatter plot showing the relationship between mean NDSI and TM band 4 reflectance for differing percent snow cover as calculated by the SCA algorithm. The numbers above each diamond indicate the range of snow cover percents used to calculate the associated means. The mean values for each

snow-cover category were calculated from Sierra Nevada TM data spatially degraded to 500 m.

14. 89-GHz passive-microwave data from transects of MIR imagery showing brightness-temperature changes from northern Alaska to southern Alaska during the April 1995 ER-2 mission. Note that not all of the flights were flown of the same areas on each day.

9.0 Appendix A

Product Level Descriptions

Level 0 - Raw instrument data at original resolution, time ordered, with duplicate packets removed.

Level 1A - Reconstructed unprocessed instrument data at full resolution, time referenced, and annotated with ancillary information, including radiometric and geometric calibration coefficients and georeferencing parameters (i.e. platform ephemeris) computed and appended, but not applied to Level 0 data.

Level 1B - Radiometrically-corrected and geolocated Level 1A data that have been processed to sensor units.

Level 2 - Derived geophysical parameters at the same resolution and location as the Level 1 data.

Level 2G - Level 2 geophysical parameters that have been gridded onto a specified Earth grid.

Level 3 - Geophysical parameters that have been spatially and/or temporally re-sampled (i.e., derived from Level 1 or Level 2 data).

Level 4 - Model output and/or results of lower-level data that are not directly derived by the instruments.

Appendix B

Responses to Reviewers' Comments from the 16 May 1996 SWAMP Land Review

Dorothy K. Hall
 Code 974
 Hydrological Sciences Branch
 NASA/Goddard Space Flight Center
 Greenbelt, MD 20771

In bold, italicized print, below are the comments, verbatim, from the SWAMP "Review of EOS -AM-1 Land Data Products for ASTER, MISR, and MODIS." Responses are shown in non-bold, regular type.

6.2.7a. Data Product: MOD10/33 Snow Cover and Gridded Snow Cover (Review based on ATBD-MOD-11 November 3, 1994, presentation at workshop, May 16, 1996, and see below)

Overview: The ATBD for the MODIS snow mapping algorithm bears the date 3 November 1994. Therefore we make the assumption that material from publications relating to developing and testing this algorithm will find its way into the next version. Otherwise, many of the serious issues raised by the last review remain unaddressed.

It is unfortunate that the reviewers used the 3 November 1994 ATBD in the current review. It is out of date. We are not aware of any 'serious issues' from the last review that remain unaddressed. Most new results from papers written since 1994 are included in the revised version of the ATBD.

a) technical/scientific soundness of the algorithm/approach described (Rating:7)

In SNOMAP, a threshold of the Normalized Difference Snow Index (NDSI) represents the foundation of the approach, with an additional threshold of band 4 (Landsat TM) reflectance to separate water. The NDSI shows similarities to NDVI in simplicity and provides a reasonable measure of snow cover for fully-illuminated open areas with optically deep snow and cover greater than about 50-60 percent. The method shows suitability for global mapping because of its automatic operation and adequate performance with fixed thresholds. The ATBD should focus specifically on global application. Other methods outperform SNOMAP on a regional scale.

The 1 November 1996 version of the ATBD (Version 3.0) focuses on global-scale applications as did the 1994 version.

This approach does not go as far as it could to capitalize on the spectral information available from MODIS; it uses one band in the visible, one band in the near IR and one in the short-wave IR. With reasonable water masks as ancillary data, this algorithm will use only two MODIS bands. Recent research developing spectral measurements for snow mapping (circa 1993) has shown that additional spectral information provides better discrimination when using threshold-type algorithms.

As stated at the 16 May 1996 presentation, we are actively planning to employ other MODIS bands for snow mapping, assuming our work with MAS data show that results are better with additional bands. Until recently, we have not had the 50-channel MAS data to work with. Therefore we did not have a way to test improvements to the algorithm.

b) value of the data product to the land science community (Rating:7).

Binary maps (on-off pixels) of snow covered are at MODIS spatial resolutions may serve the research and other interest of the Land Science community working at hemispheric and large-regional scales. Its value should improve with the availability of quantitative information on the performance of the algorithm over different land covers and terrain types.

The mixed pixel problem, as manifested in the inability of this algorithm (with the standard thresholds) to measure partial snow cover less than about 50-60 percent, represents a major concern. First, we do not know the temporal or spatial significance of partial snow cover at the global scale. Second, some areas may experience great changes in snow cover amount while never showing, to a nadir view, snow cover aerial fractions greater than 50 percent, such as forests and rugged terrain. Forests represent the primary concern.

Through a series of aircraft and field missions, we will quantify the errors inherent in mapping snow using SNOMAP in the following land covers: agricultural, alpine, forests, prairie and tundra. This will be accomplished by comparing SNOMAP-derived results from MAS data, with snow maps derived from high-resolution air photos. Though an oversimplification, initially, these errors will be extrapolated globally. Then during the post-launch time frame, when we have actual MODIS data to work with, error estimates will be refined in the following way. We will employ the 1-km resolution MODIS-derived land-cover maps to determine errors in snow-mapping in various cover types. These errors will be determined from focused field and aircraft campaigns, and from detailed comparison of the MODIS snow-cover product with the NOAA hemispheric-scale product and the NOHRSC snow maps in key areas of interest.

In the pre-launch time frame, we plan to study two methods of assessing global-scale errors in SNOMAP results:

1) Jim Foster of NASA/GSFC has shown that global albedo data (derived by Robinson and Kukla (1985) from DMSP satellite data), provide a rough measure of forest density or forest-cover fraction. Forest-cover fractions are then used to correct passive microwave algorithms for forest cover, because more snow is mapped in open areas than in forested areas, with the microwave data.

These same global albedo data can be used to identify areas of the globe in which high forest-cover density is likely to cause large errors in the measurements of snow-covered area using SNOMAP. Field and aircraft data, acquired from these areas, can confirm a problem. Once such areas are identified, and errors are quantified, a decision can be made whether or not to change the NDSI threshold within these areas in order to reduce the snow-mapping errors.

2) A global land-cover map will be employed; errors determined from field and aircraft measurements will be extrapolated globally as a rough measure of the global snow-mapping errors to be expected using SNOMAP. There is an IGBP 1-km land-cover map of North America that has 17 classes that will be used initially for error estimation. Many of the classes will be combined for our purposes in order to produce a rough estimate of SNOMAP errors globally.

Moreover, areas with snow below the detectability limit of this algorithm will cause other MODIS products to exhibit large variations. For example, surface reflectance products will show large ranges for the “no snow” condition, due to partial snow cover.

The surface reflectance product does not use snow cover as an input.

c) soundness of the validation strategy (Rating: 3)

The main weakness in the 1994 version of the ATBD and other materials reviewed lies in the quantitative validation and determination of error. Responses to the previous ATBD review acknowledge that aerial photography and methods tested rigorously against aerial photography constitute unambiguous “ground truth.” The ATBD should therefore spell out steps taken or planned to compare SNOMAP results and determine error bars for different land cover and terrain types. Limited tests with snow maps from spectral mixture modeling show the need to much more of this type of test. Too much emphasis has been placed on intercomparison of algorithms not quantitatively linked to ground truth data layers. This provides only relative measures and cannot establish absolute accuracy. The next ATBD should also describe plans to quantify algorithm sensitivity to input reflectance.

There remain serious problems with the use of the algorithm over forests, especially coniferous forests. The ATBD should 1) incorporate a detailed plan addressing

SNOMAP performance over forests, 2) make suggestions about what kinds of ancillary data layers SNOMAP would be required for use on the global scale, and 3) identify decision criteria of whether to mask out forest, at least in a pre-launch time frame.

We agree that, so far, the emphasis has been placed on intercomparison of results from different algorithms. Ideally, we want to compare the results of SNOMAP with good, high-resolution snow maps. We are attempting to do this with two data sets. The first is a data set that we acquired (high-resolution air photos) in March 1994 in Montana simultaneous with a Landsat overpass. This data set has been awkward to deal with. We are currently getting the air photos digitally 'stitched together,' so that we can construct a snow map and do a quantitative comparison with the SNOMAP-derived snow map. Additionally, we have air photos and MAS data from our study areas in Alaska, acquired during the April 1995 field and aircraft experiment. We have already run the SNOMAP algorithm on the MAS scenes. Quantitative comparison with air photo-derived snow maps will be done within the next couple of months.

Additionally, we have a field and aircraft experiment planned for next January and February in New Hampshire and Wisconsin, in conjunction with the MODIS cloud-masking (Paul Menzel, Steve Ackerman and others), and the MODIS land-cover group (Alan Strahler and Dough Muchoney of Boston University). We plan to acquire low-level air photos of sites that we will overfly with the ER-2 and the MAS. This data set will allow us to quantitatively compare the SNOMAP and air photo-derived snow maps. We hope to get a simultaneous Landsat overpass also.

The above-mentioned data sets have been and will be acquired in different land-cover types, i.e. alpine (in California and Montana), forested (in Montana, New Hampshire and Alaska), agricultural (Wisconsin), tundra (Alaska) and prairie (Montana). Using the snow maps derived from air photos, and the snow maps derived from the MAS and SNOMAP, we will be able to calculate error bars for snow mapping using SNOMAP in the various land-cover types mentioned above. These results should be available prior to the June 1998 launch of MODIS.

Use of Landsat TM for a surrogate seems suitable only for near-nadir tests, unless registered to a DEM in sloping terrain. The ATBD should describe the plan for investigating non-nadir SNOMAP product. Moreover, the ATBD should describe a plan to assess the effect on daily snow maps if significant errors were encountered at moderate viewing angles.

This is true. The TM does not contribute to our understanding of off-nadir view angle problems that may be associated with MODIS. We found that more snow is mapped in pixels at near-nadir view angles in a forested area in Canada than at far off-nadir angles. This is attributed to the forests obscuring the snow from view, especially at extreme off-nadir view angles. The off-nadir view angle problem, however, has not been noticed in

preliminary testing of the SNOMAP algorithm in non-forested, snow-covered sites in Alaska from the April 1995 MAS data set. We have included a new section in the ATBD to address this (section 4.2.3.3). Using the Alaska '95 data, we will quantify off-nadir view angle errors in tundra and forests, and develop a strategy for correcting for this effect, especially in forested areas.

d) extent to which 1994 ATBD review issues have been addressed (Rating: 3). Many of the issues raised by the 1994 review remain, especially in terms of clarity in other materials we reviewed.

We do not understand this comment. In looking over the 1994 review written by the review panel, we did very well on the validation issue, with a rating of 9/10. Quoting from the 1994 review, on validation, the 1994 reviewers stated, ***“Validation is well planned - it benefits from the efforts of a number of non-MODIS groups that are working the problem. The validation plan in the document, however, is too brief.”*** In the 1 November 1996 version of the ATBD, the validation plan is much more detailed than it was in the 1994 ATBD (see section 5.0). We have had several field and/or aircraft experiments in the past (1991 and 1992 in Montana, 1992 and 1994 in Saskatchewan, and 1995 in Alaska), and we have one planned for early 1997 in New Hampshire and Wisconsin. These field experiments are described in section 5.0 of the 1 November ATBD. Our major problem was that we did not receive any MAS data (in its 50-channel configuration) until late summer 1996. Since then we have been working hard to address validation quantitatively utilizing the MAS data.

Error analysis remains a problem. The ATBD needs much work to address both the previous review and the issues raised here.

Again, from reading the previous review, it is unclear what issues were raised in the previous review. However, we agree that error analysis should be explained better. We have added sections in the ATBD that address error analysis plans in different land-cover types (see sections 4.2.3 and 5.0). In the pre-launch time frame, using data we have already acquired, and data that we plan to acquire, we can derive error bars in our SNOMAP-derived snow maps, in various land-cover types (agricultural, alpine, forest, prairie and tundra), and extrapolate those errors to the global scale. This is discussed in section 4.2.3 of the 1 November 1996 ATBD). In the post-launch time frame, through a series of focused field experiments, we can refine the error estimates.

We suggest, as the 1994 review did, shrink lead-in material and expand and improve testing and evaluation plans.

We have deleted some lead-in material and, I believe, expanded and improved the testing and evaluation plans.

As just one example, the section discussing geographic and/or seasonal-induced error sources does not contain any detailed plan to address this issue.

This section has been deleted; in the previous ATBD, we were attempting to follow the exact section headings required by the Project. Thus there were some sections that contained very little material of substance since not all required sections were applicable to our work. We have now deleted the sections in which we had little to say.

e) near-term recommendations for improvements to the data product.

+ quantify errors with current data to determine limits of performance over different land cover and terrain types, with different viewing angles.

With the acquisition of the calibrated MAS data, we have begun to address these issues. From the Alaska '95 mission, we have MAS data in the following land covers: forests (both deciduous and coniferous), muskeg, marsh, tundra and lakes. As stated above, we now have a plan to quantify the errors of mapping snow in different land covers (see section 4.2.3).

+ place quantitative estimates on the consistency of SNOMAP performance with respect to the fractional coverage of snow required to “turn on” a pixel. This could be carried out by comparing SNOMAP, made with imagery binned to larger pixels with air photo maps, or some other reference map at higher resolution. This was suggested in the earlier review.

This has been done using SNOMAP in conjunction with Rosenthal's snow map of the Sierra Nevadas derived by spectral-mixture modeling from the 10 May 1992 TM scene. This will be done again on the additional data sets that we are working on, or plan to acquire (e.g. Montana '94, Alaska '95 and data from the New Hampshire '97 flights).

+ note that the accuracy of this product will depend on the ability to separate snow from clouds and it appears that the cloud mask product plans to use snow information. If true, how can this be done? The plan to use snow cover from a previous period will necessarily introduce substantial errors. Some clarification of this issue is needed.

The cloud mask will be initialized with snow information from the GOES satellite. Later, the Wisconsin cloud-mask developers plan to use the SNOMAP-derived maps. We will be jointly analyzing some of the data from the January/February '97 mission in New Hampshire and Wisconsin with the cloud-mask developers. We are actively involved in working together as we attend some of their meetings, and they attend ours. Ultimately, however, we have confidence that the cloud mask will do what the developers say it will do, and thus we feel that we do not have to account for clouds, except in our prototype

algorithms. Even in the prototype algorithms, we will plan to employ the Wisconsin prototype cloud-mask algorithm for testing.

f) long-term recommendations for improvements or additions to the data product

****if it becomes evident that a different algorithm could perform better than SNOMAP to produce a global product, begin to detail plans and document tests for follow-on ATBDs early, especially validation.***

Because there currently does not exist a viable alternative to SNOMAP for global use, we are not ready to do this.

****investigate the synergistic value of enhancing this data product with snow products from passive microwave sensors (SSM/I, AMSR).***

Last May, in the peer-review oral presentation, I showed several vu-graphs describing the work we've done so far using both passive MW and visible data. This was discussed in the previous and is discussed in the current version of the ATBD. Additionally, for the Alaska '95 field and aircraft program, we flew passive MW imaging sensors along with the MAS. We have always recognized the utility of using the data sets in synergy, as discussed last May, and in both versions of the ATBDs. Our '97 mission will also have passive MW imaging sensors on board. Ultimately, the optimum snow map of the future will combine MODIS and AMSR data to enable us to map snow cover and snow water equivalent. We have 3 recent papers out on this topic:

Foster, J.L., A.T.C. Chang and D.K. Hall, 1994: Snow mass in boreal forests derived from a modified passive microwave algorithm, Multispectral and Microwave Sensing of Forestry, Hydrology, and Natural Resources, 26-30 September 1994, Rome, Italy, pp.605-617.

Salomonson, V.V., D.K. Hall and J.Y.L. Chien, 1995: Use of passive microwave and optical data for large-scale snow-cover mapping," Second Topical Symposium on the Combined Optical-Microwave Earth and Atmosphere Sensing, 3-6 April 1995, Atlanta, GA.

Hall, D.K., J.L. Foster, A.T.C. Chang, D.J. Cavalieri, J.R. Wang and C.S. Benson, 1996: Analysis of snow cover in Alaska using aircraft microwave data (April 1995), Proceedings of IGARSS '96, 27-31 May, Lincoln, NE, pp.2246-2248.

6.2.7 Balance of Land Data Products as generated by EOS-AM-1 (i.e. ASTER, MISR, MODIS) to meet the needs of the broader Land science community

a) extent to which the data product (and its accuracies) is useful to the broader land science community and meshes with the other instrument data products (Rating: 4)

The snow cover extent is considered a very important product; global and regional studies have demonstrated this. The discussion on usefulness and accuracy of results from this algorithm is presented above.

Many of the other MODIS , ASTER and MISR products focus on areas of concern to the global modeling community, such as forests and mountains. These areas represent the same land conditions where SNOMAP performs less effectively. Snow in areas with cover up to 50-60% will simply not contribute to estimates of precipitation, water storage, evaporation, and so forth, through the use of this algorithm.

The statement, “*Snow in areas.....through the use of this algorithm.*” is not true. I have spoken with GCM modelers about this comment. They expect MODIS snow-cover data to be very useful. As shown in Liston (1995), the grid-averaged energy fluxes during snow melt are proportional to the fraction of the climate model grid cell that is covered by snow. The 500-m MODIS resolution represents sub-grid cell resolution for the much larger area of the GCM grid cell (e.g. 1° X 1°).

For this product, interrelationships between cloud cover and surface reflectance products need to be explicitly defined. Even small amounts of snow drastically affect results of some of these algorithms; effects should be quantified.

We cannot quantify effects in other peoples’ algorithms.

b) assessment of plans for the comparison or enhancement of similar data products from the other instruments? (Rating: 6)

Preliminary comparison with ASTER products shows progress in this direction. While we consider comparison with other products beneficial, no explicit plan has been found.

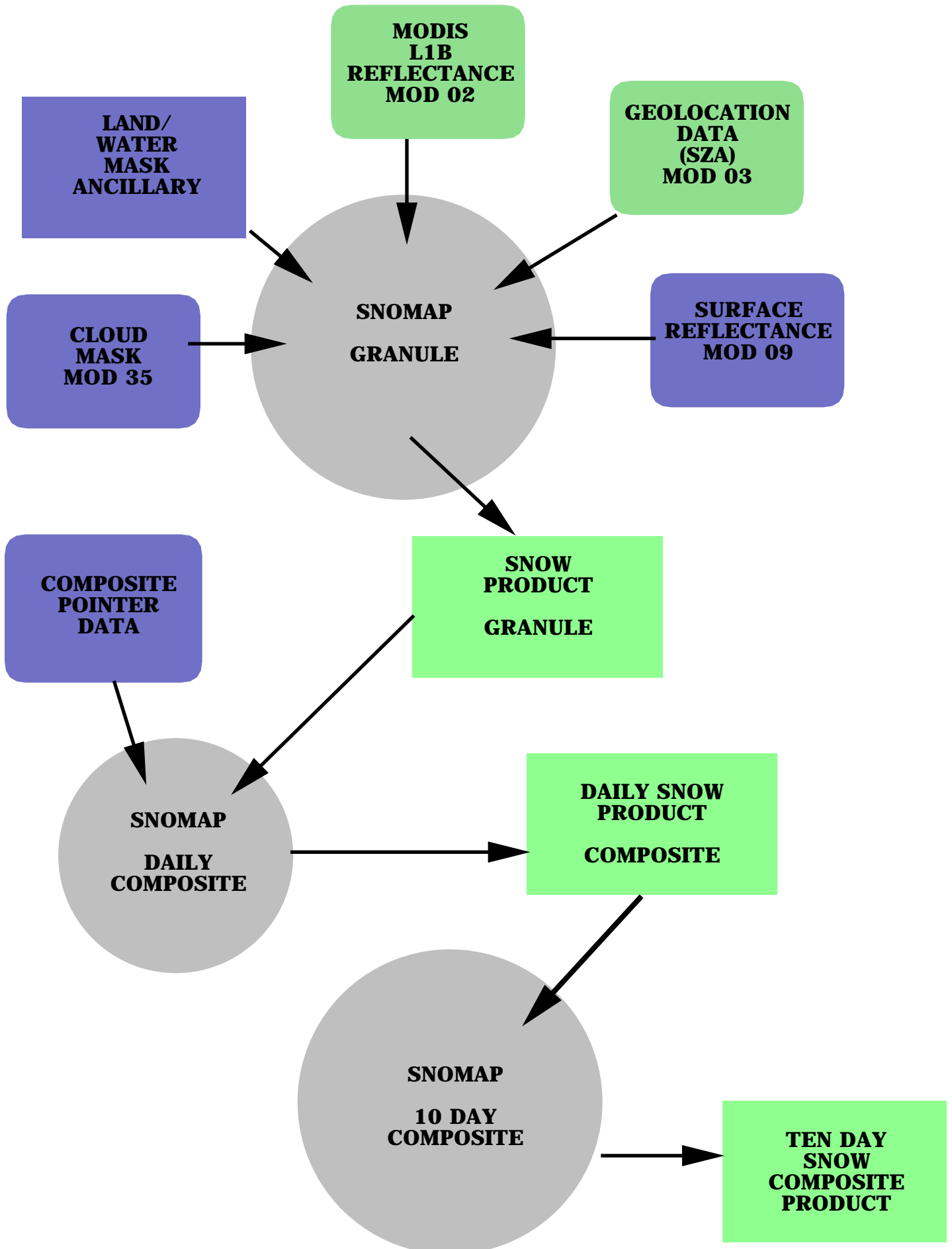
Please see 5.2 in the 1 November 1996 ATBD.

c) recommendations for changes to improve the balance of land data products
Because of the need identified above for snow algorithm improvements, initiatives a[re] recommended which expand the community involvement in this data product development.

The individuals who wrote this statement obviously did not attend the First MODIS Snow and Ice Workshop held in September 1995. Community involvement was the theme. 36 snow and ice scientists attended and most offered recommendations. All recommendations were taken very seriously. There was little consensus, but the recommendations were implemented when possible. For example, it was recommended that the MODIS snow-cover maps be produced at 500-m resolution. That change was made in the algorithm. Furthermore, an Ad-Hoc Committee on MODIS Snow and Ice

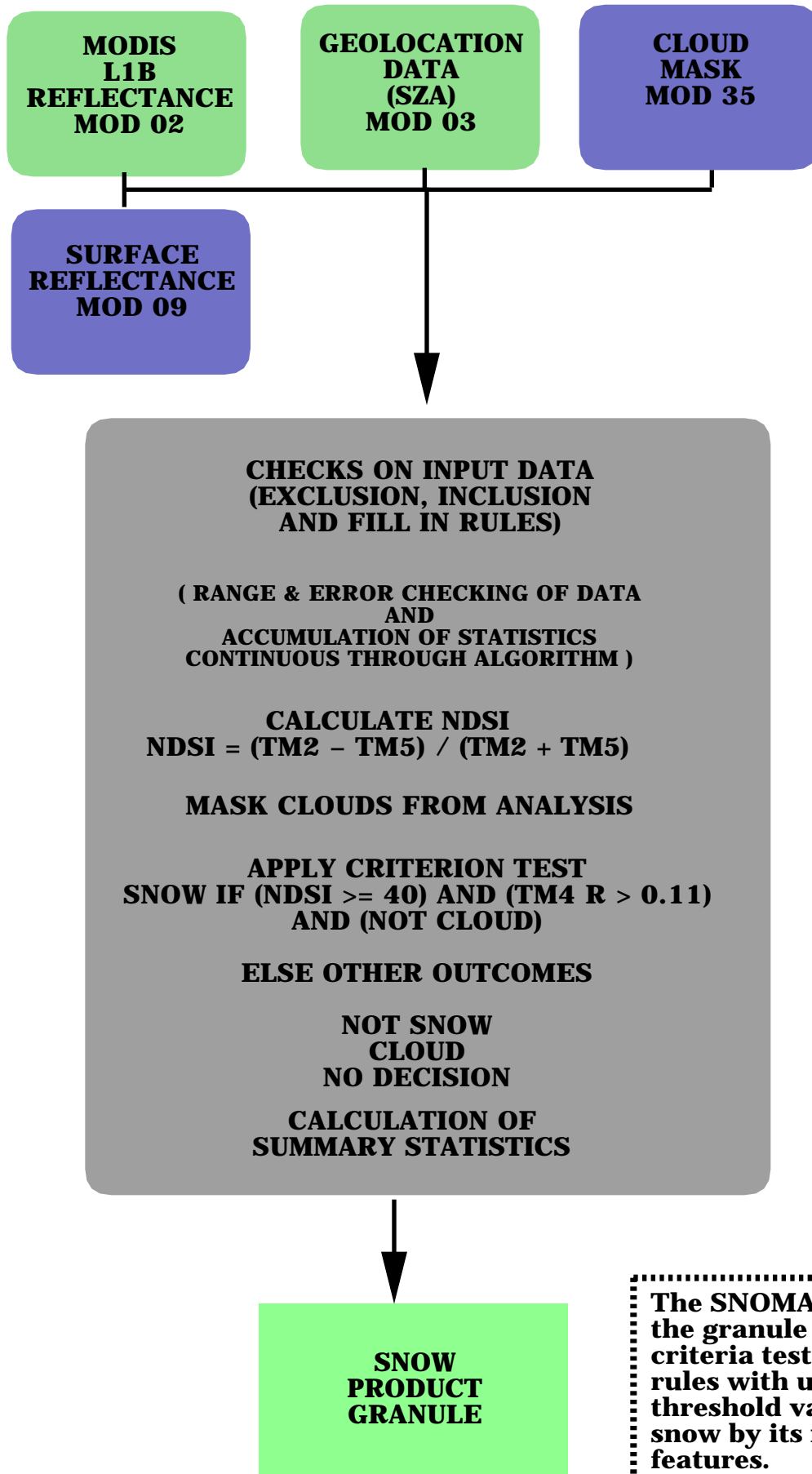
Products has been formed. The first meeting will be on November 25, 1996. Both the workshop and the ad-hoc committee were discussed during the oral part of the 16 May 1996 review.

MODIS SNOMAP FLOW



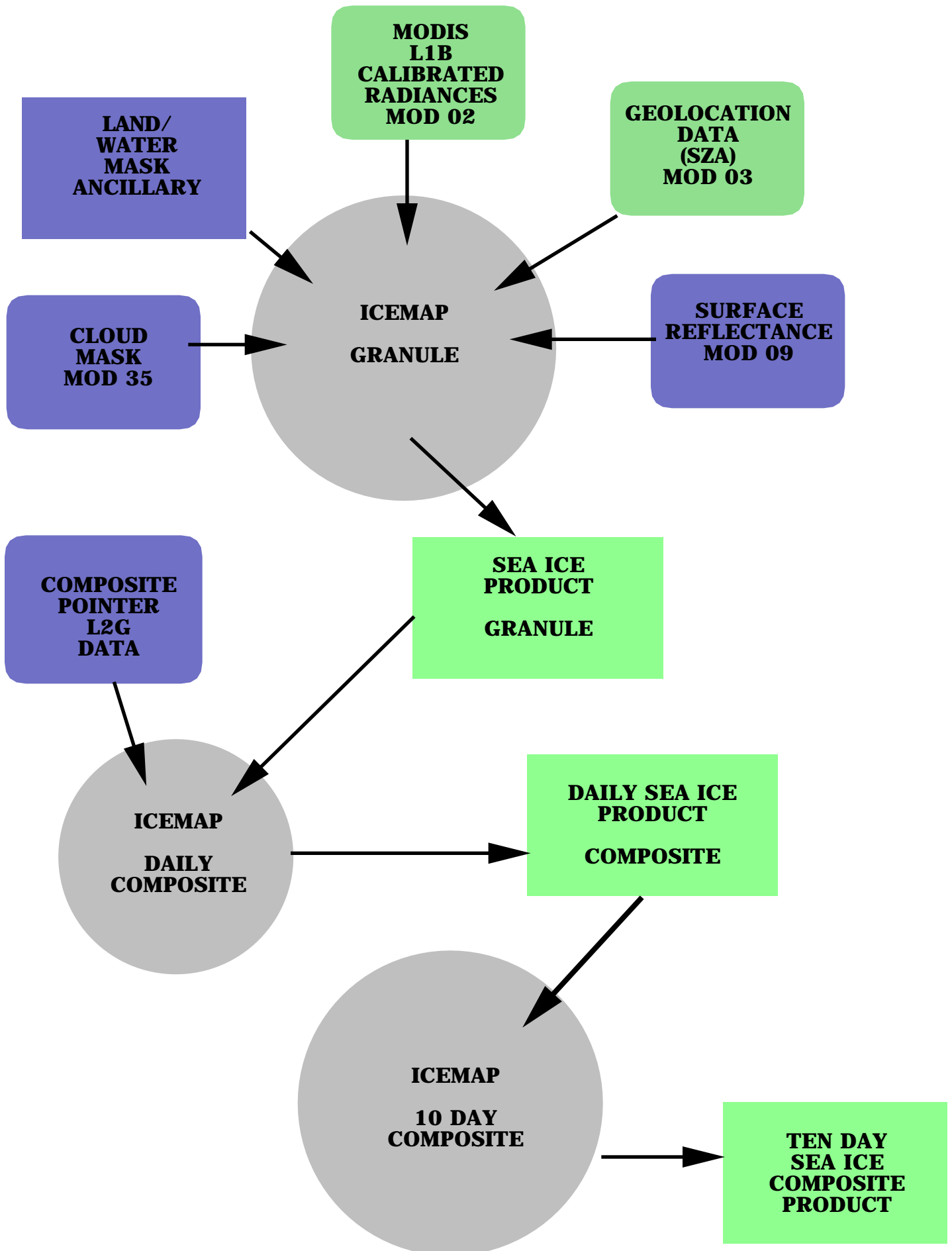
SNOMAP

GRANULE

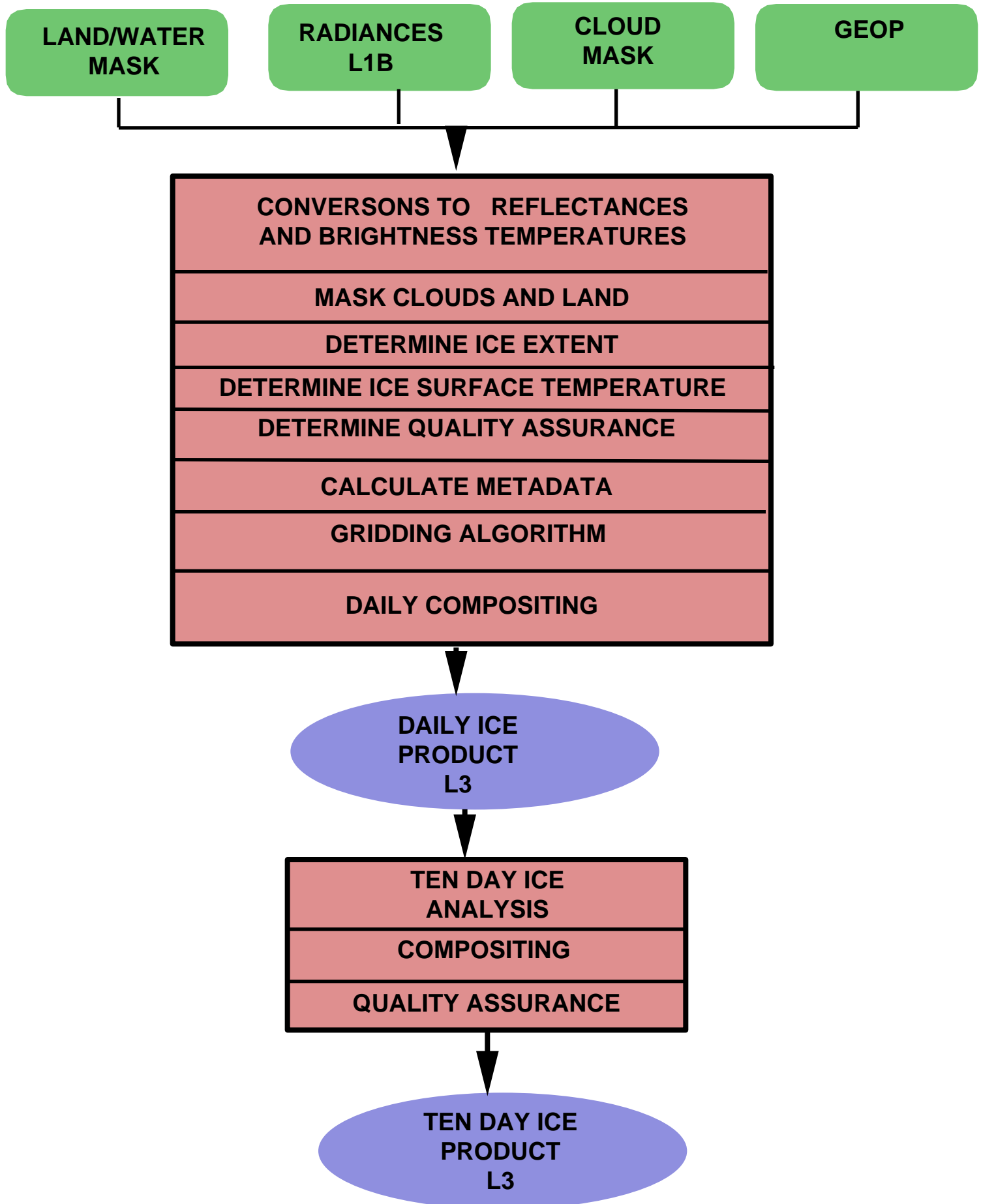


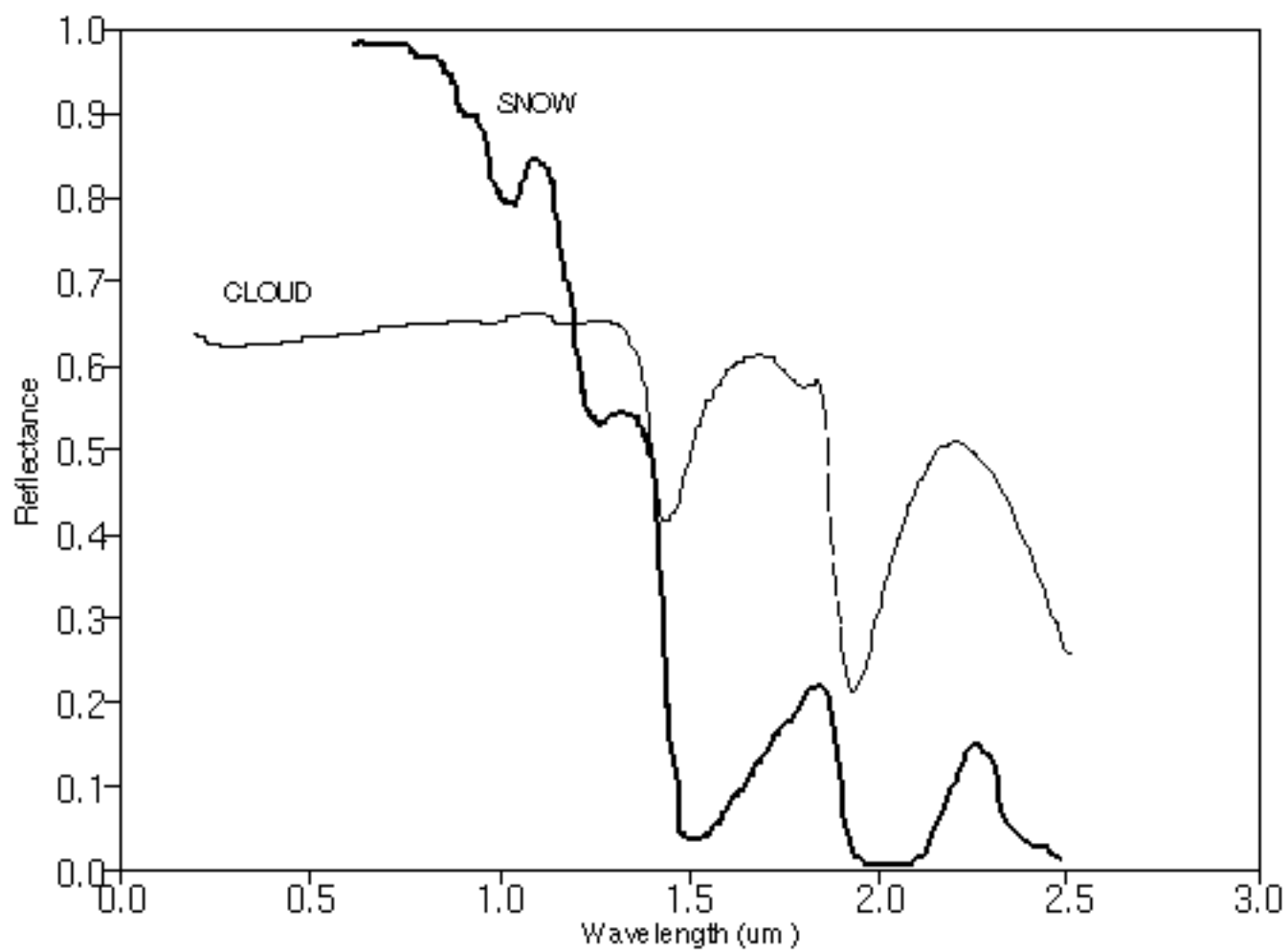
The SNOMAP algorithm at the granule level employs criteria tests and decision rules with universal threshold values to identify snow by its reflectance features.

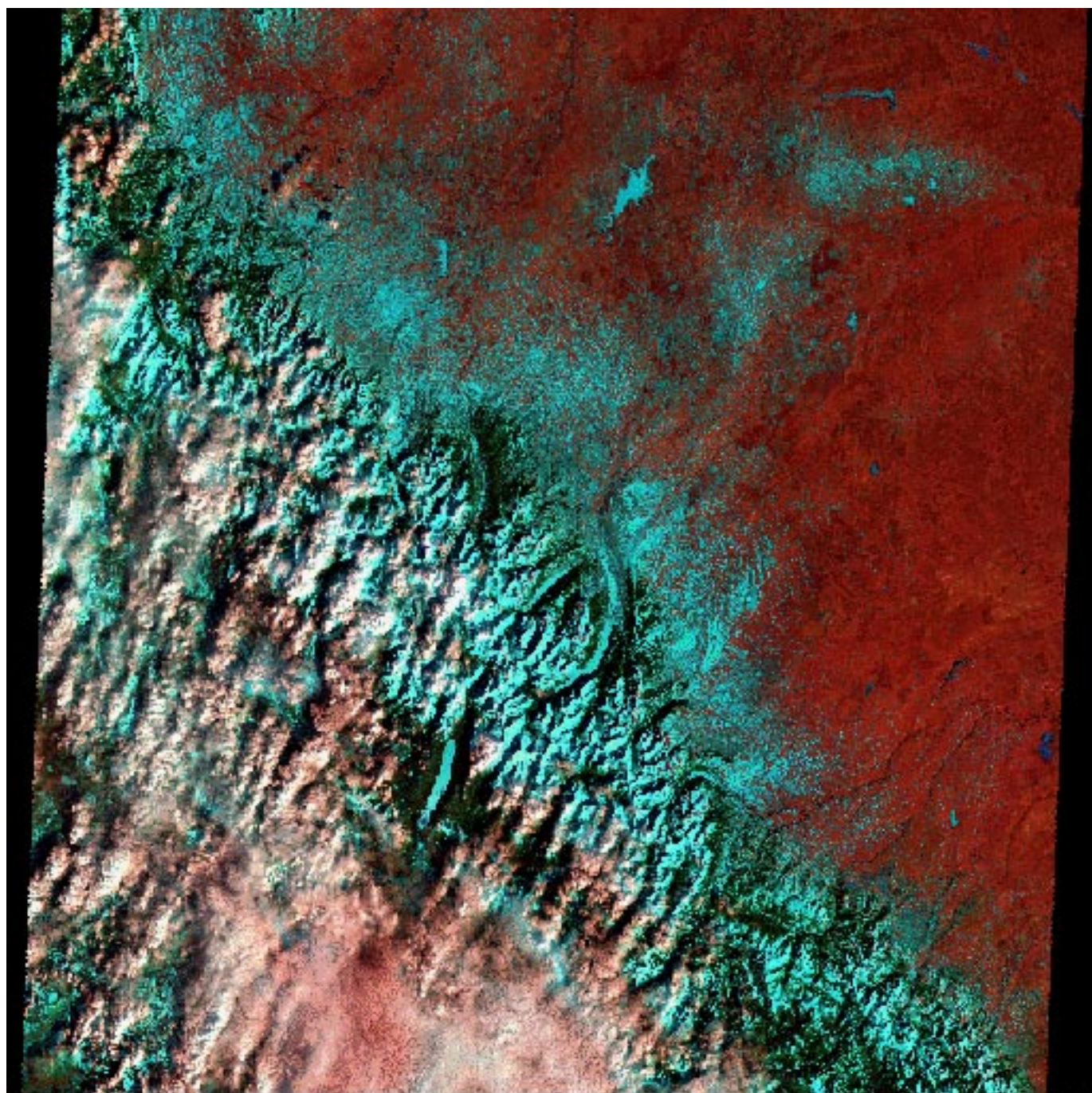
MODIS ICEMAP FLOW

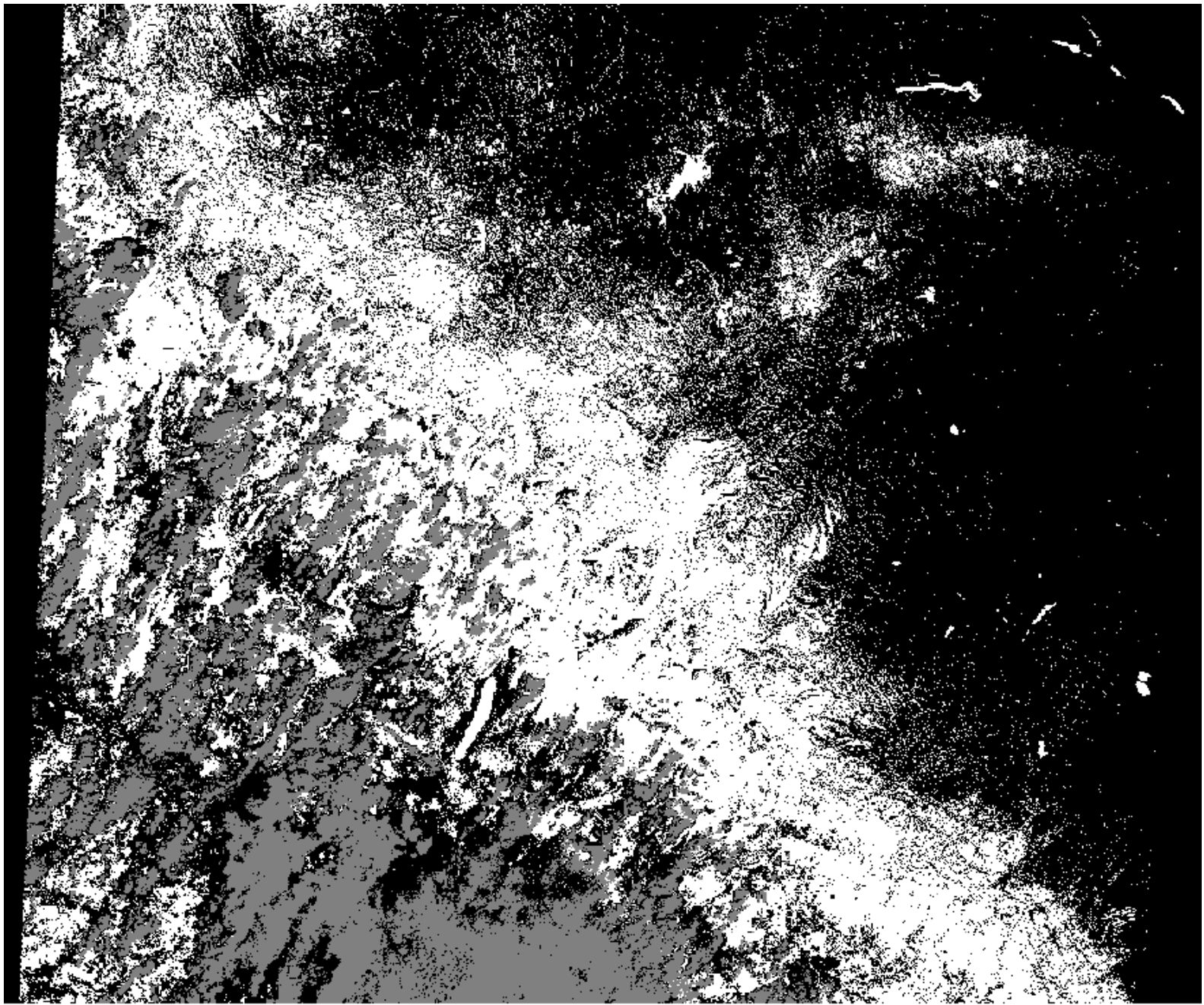


MODIS ICE ALGORITHM PROCESSING FLOW









Glacier National Park

14 March 1991



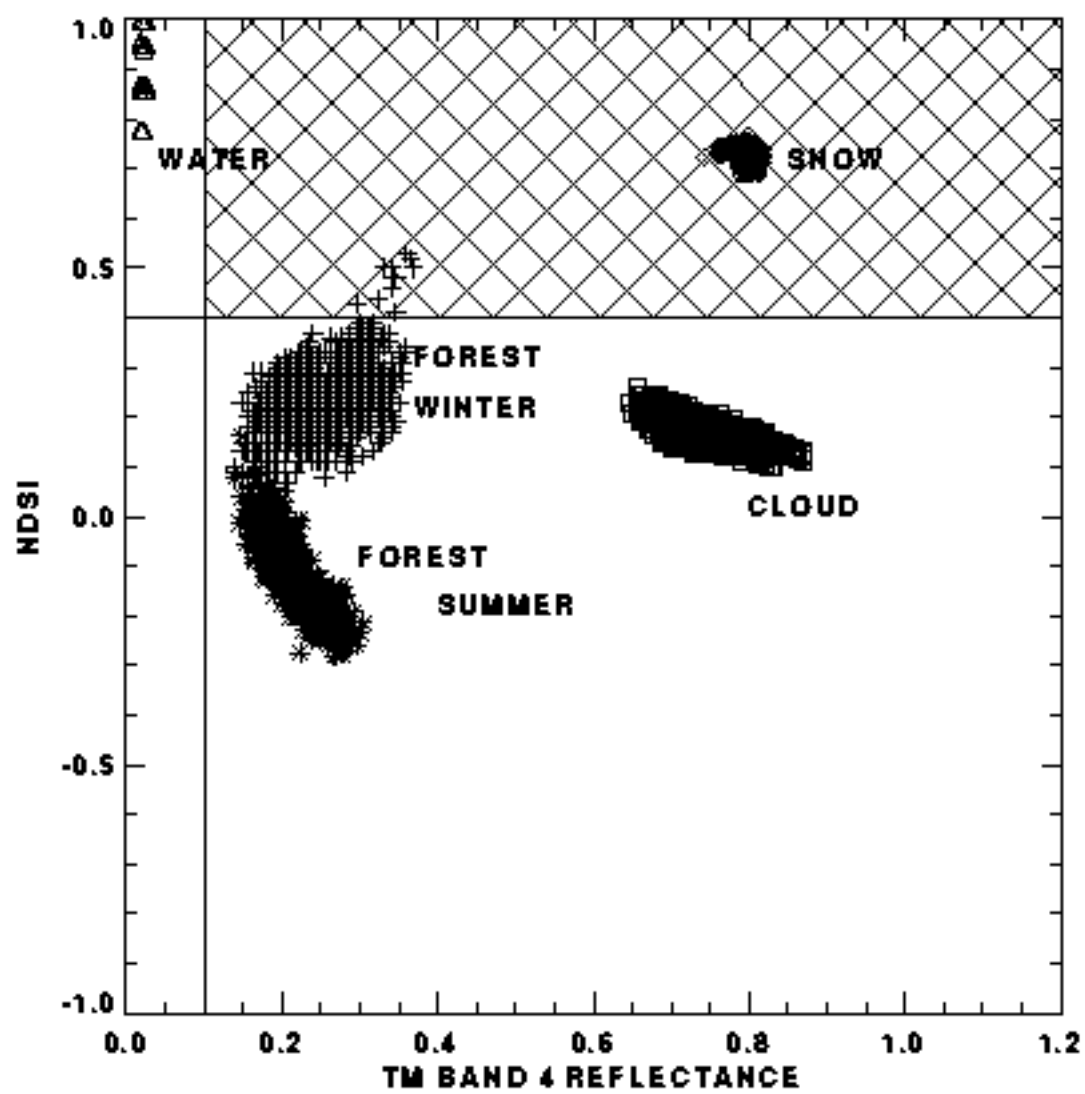
SNOW

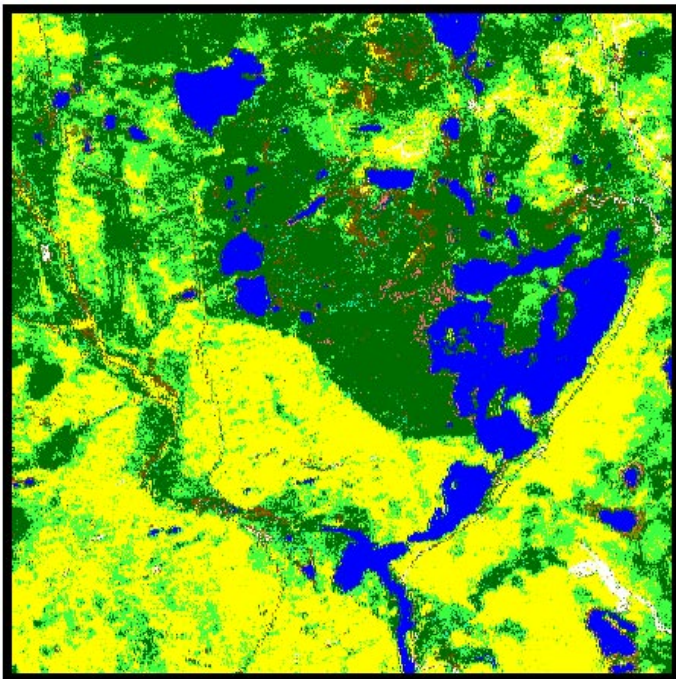


CLOUDS



OTHER





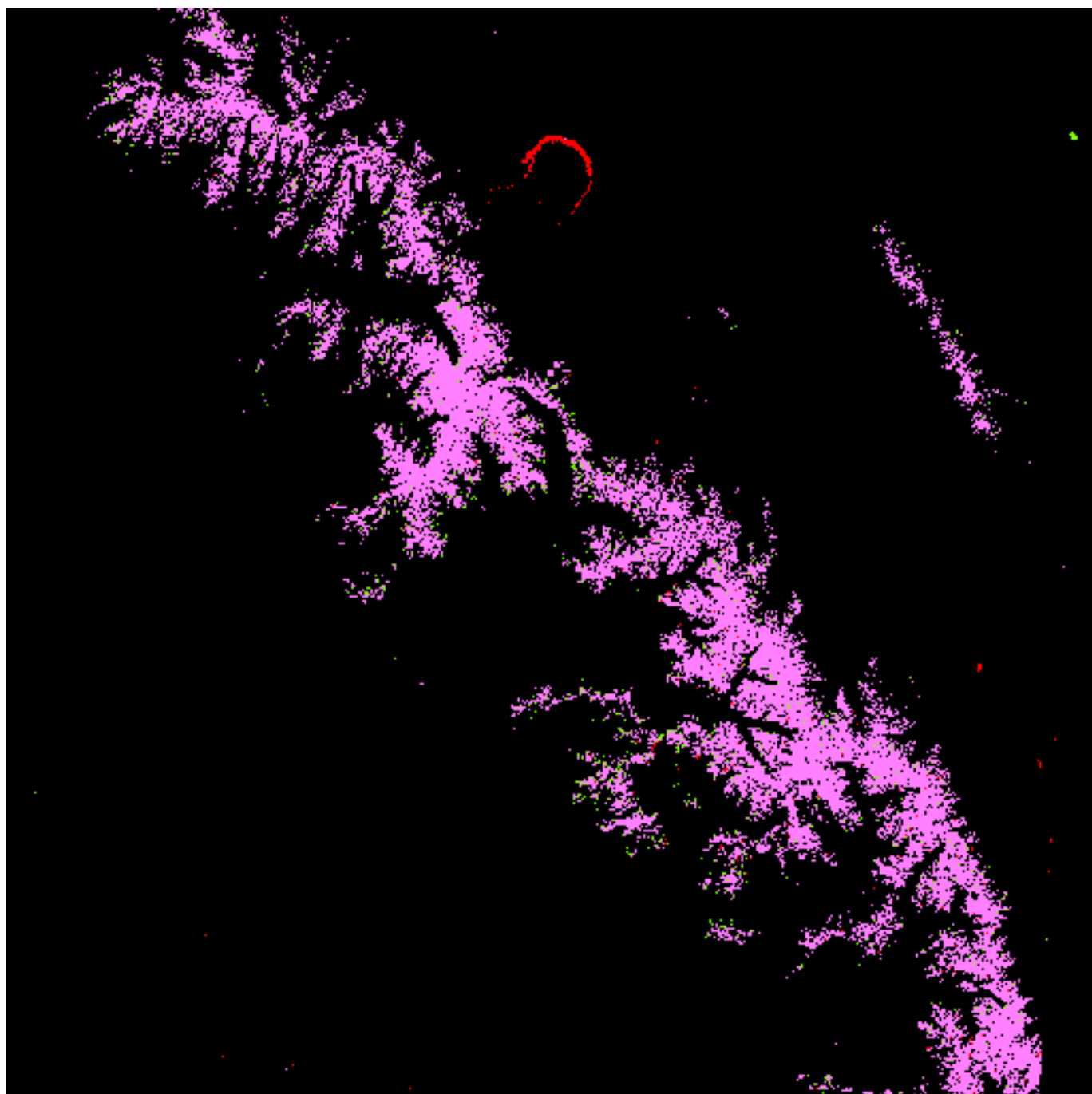
Land-Cover Classification
6 August 1990



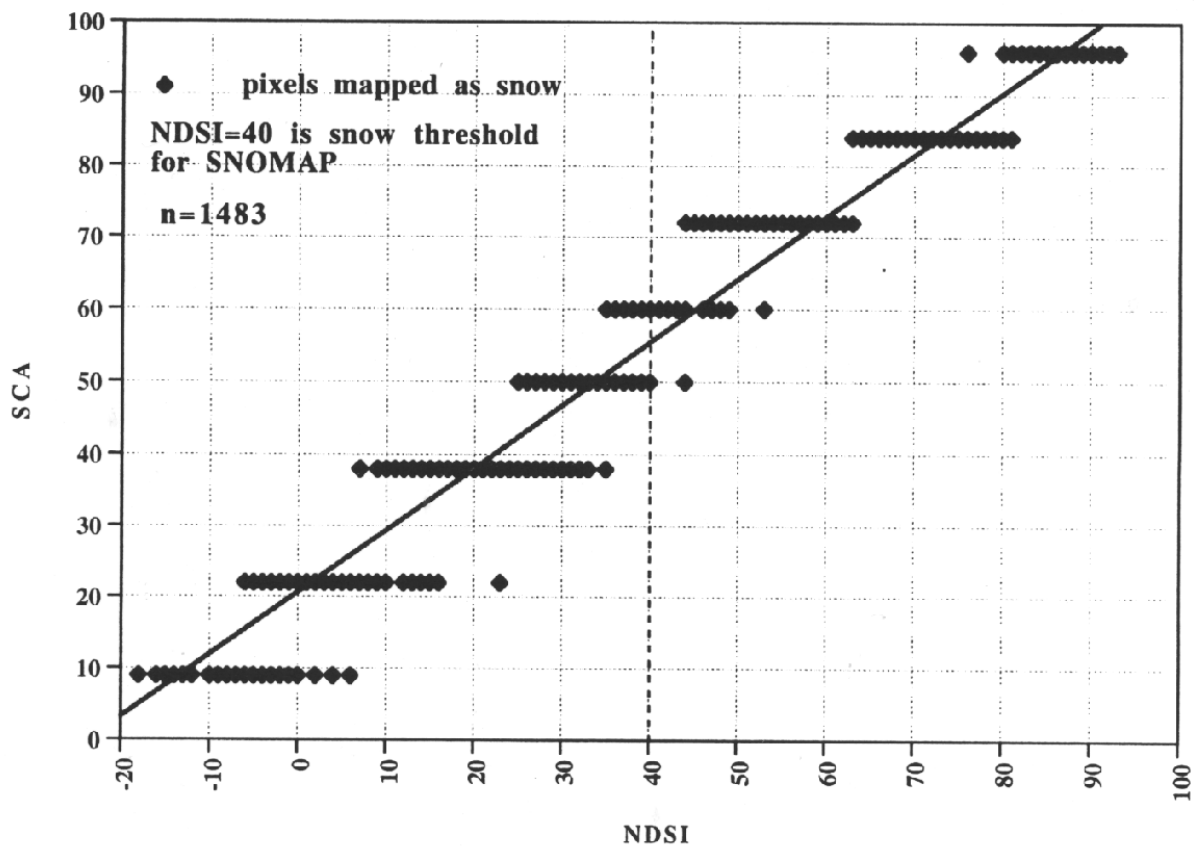
SNOMAP Result
6 February 1994

- Wet Conifer
- Dry Conifer
- Mixed Deciduous & Conifer
- Deciduous
- Fen
- Water

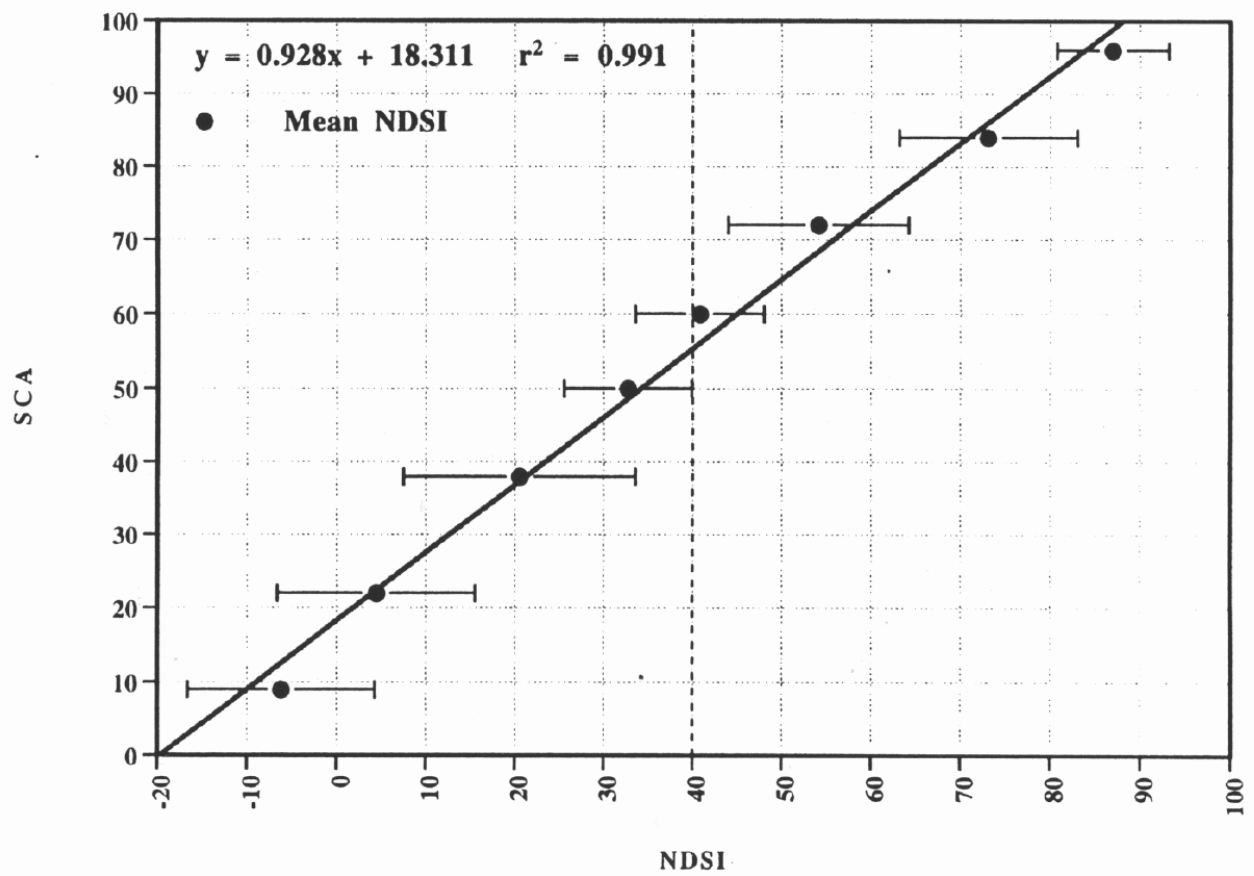
- Disturbed
- Regeneration (Young)
- Regeneration (Medium)
- Regeneration (Older)
- Visible Burn



Cross-plot of NDSI and SCA Category
- snow pixels only -



Mean NDSI v. SCA - 2stdev error bars



SCA and NDSI Techniques Compared

